The Astrophysical Journal, 839:97 (18pp), 2017 April 20 https://doi.org/10.3847/1538-4357/aa6a14

Estimates of Active Region Area Coverage through Simultaneous Measurements of the He I λλ 5876 and 10830 Lines

Vincenzo Andretta[1,5], Mark S. Giampapa[2,6], Elvira Covino[1], Ansgar Reiners[3], and Benjamin Beeck[4,5]
[1] INAF—Osservatorio Astronomico di Capodimonte Salita Moiariello, 16 I-80131 Naples, Italy; andretta@oacn.inaf.it
[2] National Solar Observatory 950 N. Cherry Avenue Tucson, AZ 85719, USA
[3] Institut für Astrophysik Georg-August-Universität Göttingen Friedrich-Hund-Platz 1 D-37077 Göttingen, Germany
[4] Max Planck Institute for Solar System Research Justus-von-Liebig-Weg 3 D-37077 Göttingen, Germany
Received 2016 July 29; revised 2017 March 24; accepted 2017 March 27; published 2017 April 20

Abstract

Simultaneous, high-quality measurements of the neutral helium triplet features at 5876 Å and 10830 Å in a sample of solar-type stars are presented. The observations were made with ESO telescopes at the La Silla Paranal Observatory under program ID 088.D-0028(A) and MPG Utility Run for Fiber Extended-range Optical Spectrograph 088.A-9029(A). The equivalent widths of these features combined with chromospheric models are utilized to infer the fractional area coverage, or filling factor, of magnetic regions outside of spots. We find that the majority of the sample is characterized by filling factors less than unity. However, discrepancies occur among the coolest K-type and the warmest and most rapidly rotating F-type dwarf stars. We discuss these apparently anomalous results and find that in the case of K-type stars, they are an artifact of the application of chromospheric models best suited to the Sun than to stars with significantly lower $T_{\rm eff}$. The case of the F-type rapid rotators can be explained by the measurement uncertainties of the equivalent widths, but they may also be due to a non-magnetic heating component in their atmospheres. With the exceptions noted above, preliminary results suggest that the average heating rates in the active regions are the same from one star to the other, differing in the spatially integrated, observed level of activity due to the area coverage. Hence, differences in activity in this sample are mainly due to the filling factor of active regions.

Key words: stars: activity – stars: magnetic field – stars: solar-type – techniques: spectroscopic

Supporting material: machine-readable table

1. Introduction

Although sunspots are the most visible manifestations of magnetic flux emergence resulting from dynamo processes, magnetic flux concentrations outside of spots in active regions form a significant fraction of the total (unsigned) magnetic flux budget of the Sun. Likewise, the total and spectral solar irradiance as functions of time cannot be modeled by considering the contribution of sunspots only (for a recent review, see Yeo et al. 2014).

Determining the distribution, or at least the fractional area coverage of magnetic active regions, is relevant to both dynamo theory and to models of chromospheric and coronal heating. With regard to the latter, flux-calibrated chromospheric emission line profiles yield the surface-averaged emission that represents a lower limit to the intrinsic emission in localized active regions. A more accurate knowledge of the actual radiative losses resulting from chromospheric heating would provide a further constraint for the development of models based on, for example, local plasma heating by Joule dissipation associated with an Alfvén wave field (Tu & Song 2013). Although information on the spatial distribution of magnetically active regions on stellar surfaces can be obtained in some special cases (mostly rapid rotators through Doppler imaging), such measurements have always been elusive in more solar-like stars.

A census of the solar magnetic flux in its various forms can be performed directly because of the distinct advantage of spatially resolved observations. In the case of stars, however, we generally rely on radiative proxies to infer the properties of the magnetic flux on the spatially unresolved stellar surface. The analogue of the solar cycle in late-type stars is typically seen through the modulation of chromospheric radiative emissions, such as in the deep cores of the Ca II resonance lines, that are spatially associated with sites of emergent magnetic fields. (Skumanich et al. 1975; Wilson 1978; Baliunas et al. 1995). The amplitude modulation of this magnetic flux is widely regarded as a property of nonlinear dynamo processes of which $\alpha - \omega$ kinematic dynamos are a particular class of mean-field dynamo models (Tobias 1997).

The high-quality photometric data from the space missions *CoRoT* (Baglin 2009) and *Kepler* (Koch et al. 2010) have yielded new insight into the rotation and magnetic properties of solar-type stars by providing rotation periods for thousands of main-sequence stars (Nielsen et al. 2013; Reinhold et al. 2013; McQuillan et al. 2014; Buzasi et al. 2016) as well as new photospheric proxies of magnetic activity based on the periodicity and amplitude of the light-curve modulation (He et al. 2015).

In order to provide a broader parameter space for the advancement of stellar and solar dynamo models, we further develop herein a method for the measurement of active region area coverages on solar-type stars (Giampapa 1985; Andretta & Giampapa 1995). In particular, we extend our previous work through the results of simultaneously acquired, high-resolution spectroscopic observations of the He I triplet lines at 5876 Å and 10830 Å, respectively.

[5] Visiting Astronomer, European Southern Observatory.
[6] Operated by the Association of Universities for Research in Astronomy under a cooperative agreement with the National Science Foundation.

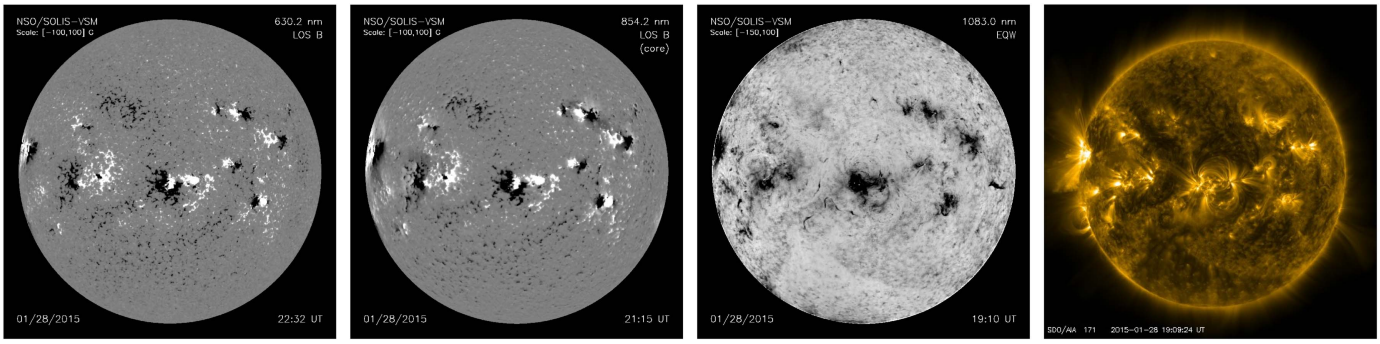

Figure 1. Full-disk images of the Sun on a date near the maximum of solar cycle 24. From left to right: longitudinal magnetograms in the photosphere (Fe I 6302 Å) and in the chromosphere (Ca II 8542 Å), a spectroheliogram in He I 10830 Å, and an EUV image of the corona at 171 Å. The first three images are from the NSF SOLIS Vector Spectromagnetograph (VSM) while the coronal image is from the Atmospheric Image Assembly (AIA) instrument on board the NASA *Solar Dynamics Observatory* (*SDO*) mission. These images illustrate the spatial correlation between localized areas of relatively strong magnetic flux in both the photosphere and chromosphere, the presence of λ10830 absorption, and the overlying coronal EUV emission. The λ10830 spectroheliogram appears more diffuse than the photospheric magnetogram, reflecting the greater height of formation in the chromosphere combined with field line spreading and the effect of EUV back-illumination.

Solar observations, such as those in Figure 1, demonstrate that these lines are ideal tracers of magnetic regions outside of cool spots, appearing in absorption in active regions and only weakly in quiet network elements and the (non-magnetic) photosphere.[7]

Thus, the measured absorption equivalent width is proportional to the active region area coverage, or filling factor (the two terms are used interchangeably in this paper), at the height of formation and the time of observation. A more precise estimate of the active region filling factor can be obtained through examination of the joint response of the He I triplet lines to chromospheric heating combined with a model-dependent calibration of the strengths that can be attained by these features in plage-like regions on the stellar surface. Recall that plages are the chromospheric counterpart of faculae, which are localized bright regions in the solar photosphere associated with concentrations of magnetic fields and characterized by reduced opacity, thus allowing us to see the deeper, hotter (and hence, brighter) walls of the facular area. The overlying plage is distinguished by relatively bright Ca II H & K emission in full-disk spectroheliograms.

We discuss in Section 2 our approach to the calibration of the joint response of the helium lines to atmospheric heating along with the results of our model calculations. The observations and their reduction are presented in Sections 3 and 4. A discussion of the inferred active region filling factors is given in Section 5. In Section 6 we present our conclusions and our anticipated directions for further research.

2. Model Approach

Andretta & Giampapa (1995, hereafter AG95) developed a technique to address this problem by demonstrating that the nonlinear response of the two main triplet He I lines (at 10830 and 5876 Å) to chromospheric heating can be exploited to infer the fractional area coverage by active regions in solar-like stars. Their approach was based on a two-component representation of the strength of activity diagnostics, where the observed equivalent width of a line, $W_{\rm obs}$, can be written in terms of the contributions from the quiescent atmosphere, $W_{\rm q}$, and the active (plage-like) atmosphere, $W_{\rm a}$, via a filling factor f, where

$$W_{\rm obs} = (1 - f)\,W_{\rm q} + f\,W_{\rm a}. \quad (1)$$

Further details on the derivation of the above equation can be found in AG95. We only note here that the difference in continuum intensities between the quiescent and active atmosphere is assumed to be negligible. At this level of approximation, this is a valid assumption in the Sun and by analogy, in solar-type stars.

In the two-component model described above, the quantities $W_{\rm q}$ and $W_{\rm a}$ represent the *average* values in the quiescent atmosphere and in active regions, respectively. In both regions, the observed line strengths can of course vary on smaller scales. In the quiet Sun, for example, chromospheric line strengths are typically distributed in a characteristic spatial pattern called the "supergranular network." The main assumption of Equation (1) is therefore that the average value of the strength of the activity diagnostics, $W_{\rm a}$, is the same in all active regions on the stellar surface independent of their area, i.e., small and large active regions are equally "bright" when imaged in the chosen activity diagnostics. Figure 1 shows that this assumption is plausible, but for most activity diagnostics this assumption can also be quantitatively verified (e.g., Andretta & Del Zanna 2014).

In this approach, the filling factor, i.e., the fractional area covered by active regions, is therefore one of the fundamental parameters discriminating between stars with different observed activity levels. In the favorable case of a negligible contribution from the quiescent atmosphere, the filling factor is simply $f = W_{\rm obs}/W_{\rm a}$. But even in this case, the filling factor cannot be determined unless the intrinsic line strength in stellar active regions is known. AG95 showed that this ambiguity can be resolved by observing two lines with different, nonlinear dependences on the atmospheric activity.

In order to apply the method described by AG95 to a pair of activity diagnostics such as the main He I triplet lines, the dependence of the intrinsic strength of both lines on the active region heating needs to be computed, $W_{\rm a}(p)$, where p is a parameter, or set of parameters, characterizing the active regions in the formation layer of the diagnostics under consideration. In AG95, the activity parameter is the mass loading, or column density, m, in g cm^{-2} at the top of the chromosphere or equivalently, the increase of total chromospheric pressure relative to the quiescent state, $P/P_{\rm q}$. A more

[7] See Harvey et al. (1975) for an analogous figure that includes more rare spectroheliograms in He I λ5876 (D_3) obtained simultaneously with solar X-ray images from *Skylab*.

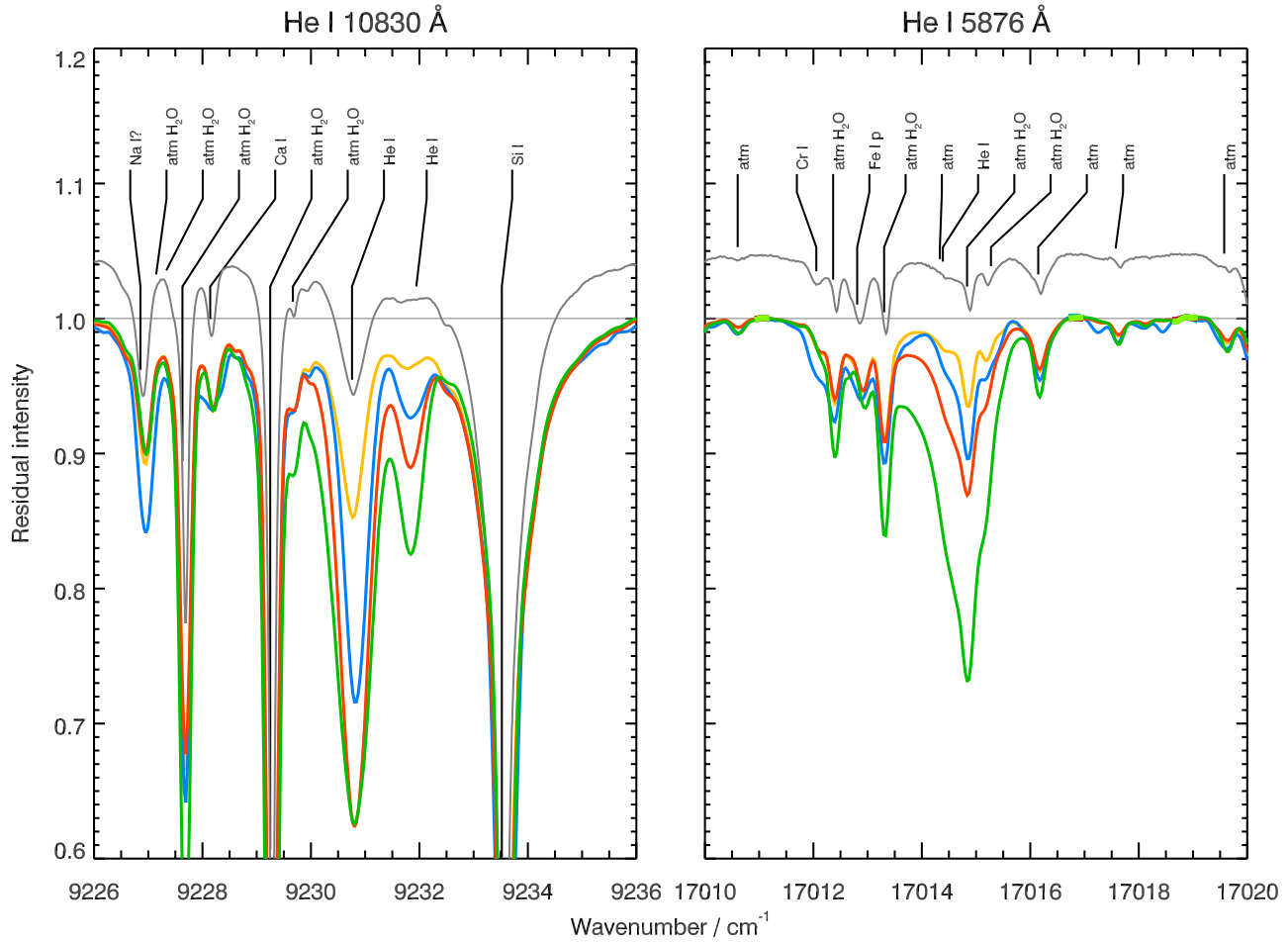

Figure 2. Solar observations of the He I triplet lines in various locations of an active region. The data were obtained on 1995 March 16 with the Fourier Transform Spectrometer at the NSF McMath–Pierce Solar Telescope on Kitt Peak (Brault 1979). The spectra refer to various locations of plages or plage-like areas of AR 7854. On the left and right panels are marked, respectively, the He I lines at 10830.3 Å (air wavelength, corresponding to wavenumber 9230.8 cm^{-1}, with its minor fine structure component at 10829.0 Å, or at wavenumber 9231.9 cm^{-1}) and at 5875.7 Å (corresponding to wavenumber 17014.5 cm^{-1}). In both panels, the nearest solar and telluric lines are also marked, including the group of telluric water lines within the profile of the He I λ5876 feature. The reference solar flux atlas by Kurucz et al. (1984) is also displayed for comparison (gray) with an offset of 0.05 above the observed spectra.

complete set of activity parameters can be considered, as described below.

In comparison with other diagnostics, the helium triplet lines are especially suitable for this approach since they respond to chromospheric heating, which is parameterized in model computations by higher chromospheric pressure in the line formation region, by increasing their absorption equivalent widths in a nonlinear fashion (see AG95, their Figure 2). At sufficient densities, such as those that may occur in a flare, collisional control eventually overcomes scattering processes and the triplet lines are driven into emission. Thus, as atmospheric heating increases, all He I triplet lines go deeper into absorption, reaching a maximum in their equivalent widths before eventually going into emission.

This general behavior of the helium lines is in qualitative agreement with observations, as illustrated in Figure 2, where we see varying strengths in the triplet lines at different locations in a solar active region, presumably in response to different degrees of chromospheric heating.

We note that this behavior is very much reminiscent of Hα line formation in the chromospheres of M dwarf stars (Cram & Mullan 1979; Giampapa et al. 1982). Following the approach of Giampapa (1985), the existence of a maximum in intrinsic line strength in active regions, W_{max}, can be exploited to derive a lower limit to the filling factor:

$$f \geqslant \frac{W_{obs} - W_q}{W_{max} - W_q}, \quad (2)$$

or if $W_q \approx 0$, $f \geqslant W_{obs}/W_{max}$.

The key point of the method described in AG95 is, however, that each line attains its maximum equivalent width at different amounts of atmospheric heating. This leads to a strongly nonlinear joint response of the line strengths. Thus, simultaneous observations of two lines can in principle allow an unambiguous determination of the filling factor *f*. This behavior is illustrated in Figure 2, where the main component of the λ10830 line seems to reach a level of "saturation" in its equivalent width while both the D_3 line and the minor component of the IR triplet line at 10829 Å continue to increase in their strength.

The essence of the method is illustrated in Figure 3, which displays theoretical diagrams as calculated by AG95 of the joint response of the triplet lines in equivalent width to chromospheric heating (dotted–dashed lines), together with the set of calculations adopted here and described in Section 2.1 below. The locus $f = 1$ defines a region (highlighted in solid

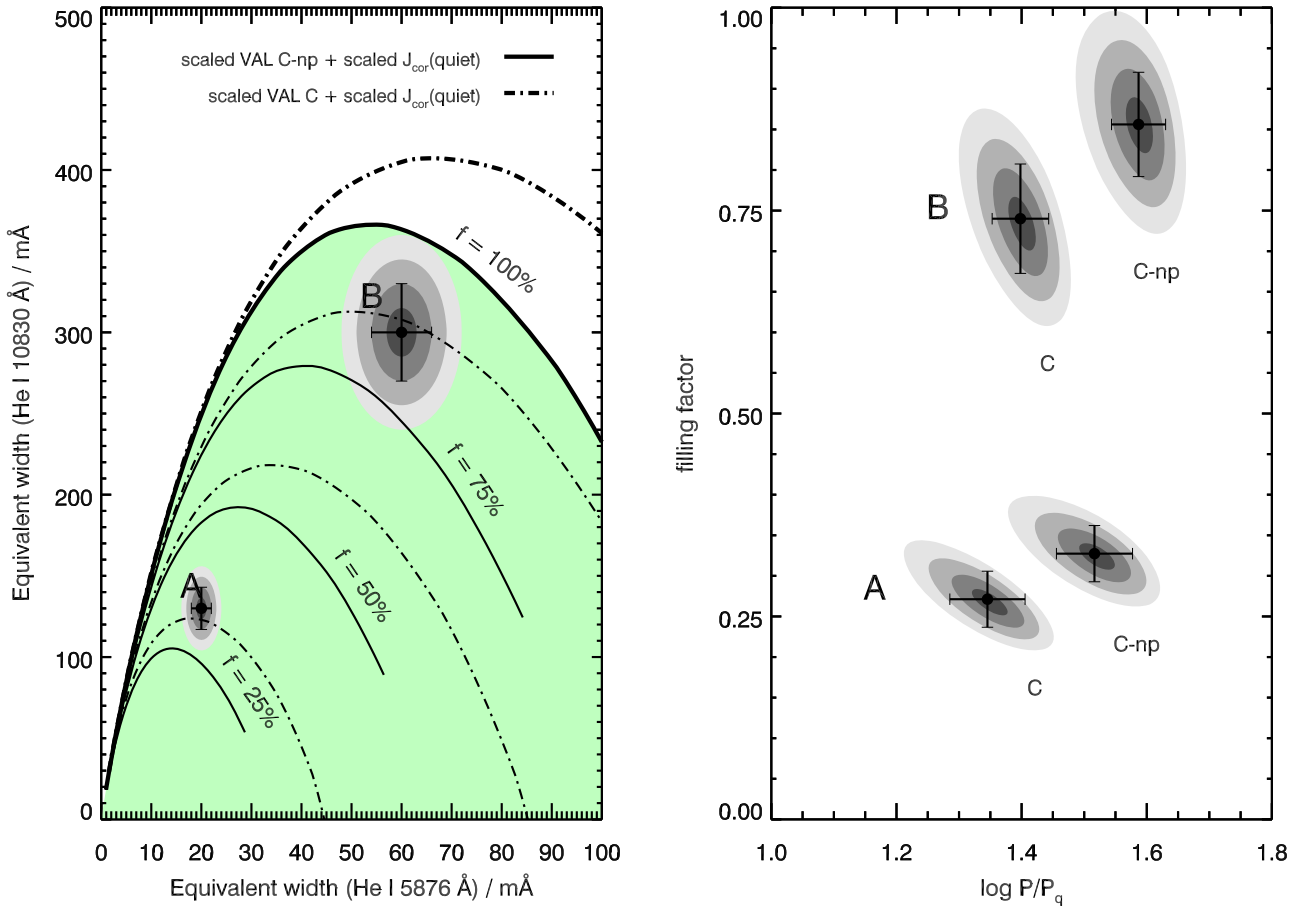

Figure 3. Illustration of the method described in AG95 in the case of the joint response of the main He I triplet lines. Two hypothetical observations, labeled A and B, are also shown to illustrate the effect of uncertainties in the equivalent width measurements on the determination of the filling factor by this method. The error bars and the corresponding bi-dimensional probability distribution in the left-hand panel correspond to a 10% uncertainty in both equivalent widths. The transformed distributions in the $(P/P_q, f)$ plane are shown in the right-hand panel for the two series of theoretical models, labeled C and C-np, that are described in Section 2.1 and shown in Figure 4. The dots and error bars represent, respectively, the mean and standard deviation of the transformed distributions of the filling factor and pressure enhancements.

color in the figure for the reference calculations) where all measurements should fall; it was already shown in AG95 that observations of solar-like stars do indeed fall in this allowed region. We also note that to infer the filling factor, it is not necessary to have detailed knowledge of the specific activity state of the stellar plage-like regions, but only of the joint dependence of the two spectral diagnostics. Nevertheless, the values of the activity parameter p that best match the observations can still be derived together with f by inverting Equation (1) for the selected activity diagnostic pair.

The effect of measurement errors is also shown in Figure 3. Two hypothetical joint measurements of λ5876 and λ10830 with a 10% (1σ) uncertainty are shown in the left-hand panel of that figure. The corresponding bi-dimensional probability distributions are shown as filled gray contours. In the right-hand panel, the probability distribution transformed by the inversion of Equation (1) for both lines is shown in the $(P/P_q, f)$ plane for both sets of theoretical calculations of $W_a(P/P_q)$ we have considered and that are discussed in Section 2.1 below. The mean value and the standard deviation of the transformed distributions are shown as error bars. In particular, the mean and the standard deviation of the transformed probability distribution for the filling factor are its value and error we will attach to the actual measurements described in the remainder of this work.

In addition to the general properties of their joint response to chromospheric heating, the helium triplet lines exhibit several desirable features:

1. they are purely chromospheric lines: the photospheric contribution to these lines is negligible in solar-like stars;
2. their strength in the quiescent chromosphere is small: the observed lines in spectra of solar-like stars arise almost entirely in active regions: $W_q(D_3) \approx 0$ and $W_q(\lambda 10830) \approx 40$ mÅ (the latter value is inferred from full-disk measurements during the minima of solar activity: Harvey & Livingston 1994; Livingston et al. 2010);
3. they both belong to the same atom: therefore, the effect of the elemental abundance is largely factored out;
4. the transitions giving rise to the two lines share one atomic level ($1s2p\ ^3P$) in so-called orthohelium: thus, their differential behavior is relatively insensitive to the details of interactions with other atomic levels; and
5. they form essentially in the same zone of the chromosphere, regardless of the details of the formation mechanism (Andretta et al. 1995; Andretta & Jones 1997). Hence, they probe exactly the same regions of the stellar atmosphere.

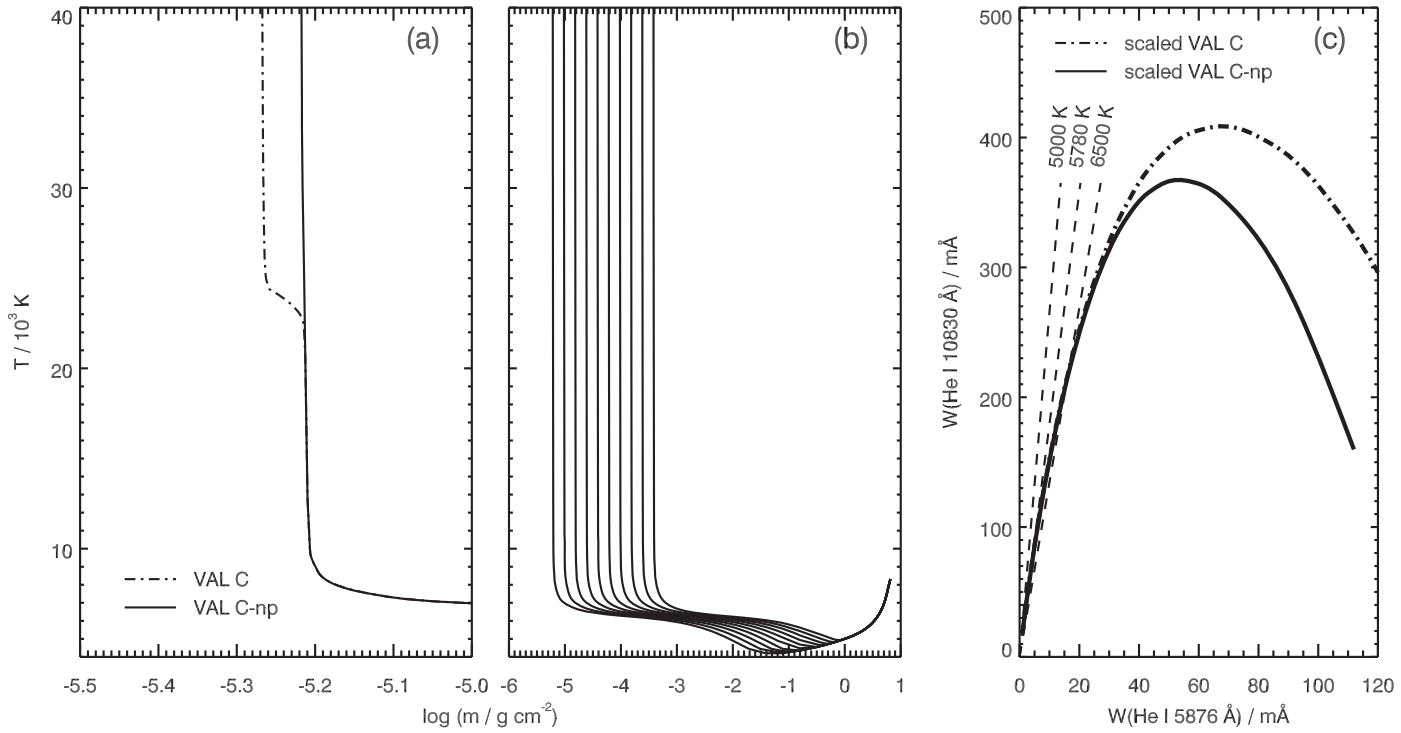

Figure 4. Model calculations. (a) Two examples of quiescent model chromospheres from AJ97 in temperature vs. mass column density, m. (b) The series of models derived from the VAL C-np quiescent model by increasing the mass loading at the top of the atmosphere. (c) The computed theoretical diagrams of $W(\lambda 10830)$ vs. $W(D_3)$ at $f = 1$, for a star with $T_{\rm eff} = 5800$ K. The optically thin limit of the joint response of the two lines is also shown by the dashed lines as functions of stellar effective temperature. See Section 2.1 for a detailed description of the models.

2.1. Reference Calculations

In AG95, the atmospheric activity level is parameterized by the column density, m, in g cm^{-2} at the top of the chromosphere. This formulation has the advantage that the total chromospheric pressure, P, is simply given by $P = gm$, where g is the stellar surface gravity. Implicit in this relation is the assumption that the chromosphere is thin with respect to the stellar radius. In a parallel study, Andretta & Jones (1997, hereafter AJ97) carried out a more extensive analysis of the parameters determining the formation of the helium spectrum in the Sun.

The reference quiescent model adopted in both AG95 and AJ97 is the VAL C model of the quiet Sun (Vernazza et al. 1981). In AJ97, two modified versions of the model, termed VAL C-np and VAL C-nt, were also considered, which differ from the VAL C model only in the thickness of the transition region, Δh(TR). The C-nt series, i.e., the series starting from the VAL C-nt model, was used in AJ97 only to discuss some specific radiative transfer aspects of the line formation; we will not consider this series of models here.

Both AG95 and AJ97 included in their analysis the effect on the helium ionization balance of the coronal EUV back-illumination integrated in the range $\lambda < 500$ Å ($J_{\rm cor}$). In AG95, the EUV back-illumination was suitably scaled to account for the increased coronal emission in active regions. The same scaling was also applied by Andretta (1994, hereafter A94) for the C-np series of atmospheric models. Hence, the pair $\{m/m_{\rm q}, \Delta h({\rm TR})\}$ constitutes the fundamental set of parameters, p, determining both the structure of the atmosphere and the coronal back-illumination, that, in turn, are used to compute the theoretical equivalent widths of the He I triplet lines to be used in Equation (1), $W_{\rm a}(p)$.

In AJ97, it was shown that the C-np series, i.e., the series of atmospheres with a reduced temperature plateau at $\approx 2 \times 10^4$ K, matches the observed properties of the solar He I spectrum better than the C and C-nt series, from the extreme UV (EUV) to the IR. That finding is consistent with the structure of solar plages derived from semiempirical models (e.g., Fontenla et al. 1993, 2006). We therefore adopt the C-np series as our reference set of models, considering however the scaling of EUV back-illumination as computed by A94 and AG95. We nevertheless also take into consideration the C series of models, i.e., the series based on the VAL C model, as in AG95, for comparison. Figure 4 shows the series of models computed in A94 (panels (a) and (b)) which were then employed by AG95, AJ97, and in the present work, together with the corresponding joint response of the triplet lines as functions of the parameter $P/P_{\rm q}$ (panel (c)).

The effect of the choice of the series of models on the determination of the filling factors is illustrated in Figure 3. For the two examples shown, the differences introduced by the different theoretical calculations of $W_{\rm a}(P/P_{\rm q})$ are larger than the uncertainties due to measurements errors, if the latter are of the order of 10% or less.

We note, however, that the maximum equivalent width attained by the He I λ10830 line is very similar in the two series of models: $\approx$370 mÅ for the C-np series and $\approx$410 mÅ for the C series. From an observational point of view, Sanz-Forcada & Dupree (2008) noted that data for cool dwarfs and subdwarfs tend to be below those theoretical limits, with very few exceptions in very active binaries. A similar result is obtained by inspecting the data of Zarro & Zirin (1986).

Regarding the quiescent value for the He I λ10830 line adopted here ($W_{\rm q} = 40$ mÅ), we note that data published in Zarro & Zirin (1986) for low activity stars for which some He I

λ10830 absorption could be detected tend to cluster around ∼50 mÅ (see their Figures 1 (a) and (b)). Values reported by Takeda & Takada-Hidai (2011) have a median of 35 mÅ, while values reported by Smith et al. (2012) are around ∼30 mÅ. These last two papers present mostly data for low-metallicity, low-gravity stars whose atmospheres could significantly differ from those of solar-like stars as far as the relevant regions contributing to the formation of the He I optical lines are concerned (photosphere, transition region, corona.) Furthermore, the relatively modest variations in the minimum detected λ10830 equivalent width have little effect on the values obtained with Equation (2), since $W_{\max}$ is about an order of magnitude larger than W_q.

In conclusion, the lower limits of the filling factors derived from Equation (2) are practically insensitive to the details of the adopted models. On the other hand, the D_3 line never attains its maximum in the grid of models considered by AG95 and AJ97 and therefore a similar approach based on D_3 measurements alone is not feasible in solar-like stars.

Concerning the dependence of the joint response of the He I triplet lines on stellar effective temperature, the calculations of AG95 for an F star with $T_{\rm eff} = 6500$ K show a slightly lower slope of the initial linear part of the curve compared to the case of the Sun, considered as a typical G-type star. This behavior can be understood given that at low activity levels, the line formation is dominated by scattering of photospheric radiation (see discussion in A94 and AJ97). The relevant photoexciting radiation determining the slope of the linear part of the joint response of the λ10830 and λ5876 lines is the photospheric radiation field at 10830 Å. Following the same argument, we expect calculations for chromospheres illuminated by the photosphere of a K-type star to show a slightly steeper joint response of the two triplet lines at low activity levels. The effect of the photospheric radiation on the joint response of the two He I triplet lines is shown in Figure 4 for the optically thin case.

Finally, we note that a number of theoretical and observational studies on the formation of the helium spectrum in the Sun have appeared since A94, AG95, and AJ97 (e.g., MacPherson & Jordan 1999; Andretta et al. 2000, 2003, 2008; Smith & Jordan 2002; Smith 2003; Judge & Pietarila 2004; Pietarila & Judge 2004; Mauas et al. 2005). Most of those studies, however, were focused on the formation of the EUV lines and continua, while the mechanism responsible for the formation of the optical subordinate lines has attracted comparatively less attention, with some recent exceptions such as Leenaarts et al. (2016). In any case, we remark that in this investigation we are merely utilizing those earlier calculations, and that updating the models is beyond the scope of this paper.

3. Observations

Given the potential effects of variability due to magnetic activity on the strengths of the triplet features, combined with a method based on observations of the joint behavior of these diagnostics, our observational approach was to obtain spectra of the D_3 line in the visible and the near-infrared (NIR) λ10830 line on the same night, respectively. Obtaining simultaneous spectra of the two lines is a challenge even in the case of the Sun, but it is nevertheless feasible, as the spectra of Figure 2 demonstrate. In addition to those FTS spectra, to our knowledge only Muglach & Schmidt (2001) have been successful in obtaining simultaneous observations in the two lines. On the other hand, we could not find analogous observations of solar-like stars in the literature, although both the He I λ5876 and the λ10830 lines have been extensively studied in the context of stellar activity, as we briefly recap in the following.

Guided by He I D_3 spectra obtained for solar plages (Landman 1981), extensive stellar observations of D_3 as an activity diagnostic utilizing digital detectors with peak sensitivities in the visible soon followed. Lambert & O'Brien (1983) reported the detection of rotational modulation of D_3 in selected main-sequence stars. Wolff & Heasley (1984) conducted a survey of D_3 in a sample of G and K stars followed by a survey focused on main-sequence stars (Wolff et al. 1985). These investigations were soon followed by focused studies addressing specific questions. Examples include the determination of the effective temperature on the main sequence corresponding to the onset of chromospheric activity associated with outer envelope convection (Wolff et al. 1986; Wolff & Heasley 1987; García-López et al. 1993); the correlation of D_3 absorption strength with rotation as well as its empirical relationship with other diagnostics of magnetic-field-related activity such as X-ray emission (Saar et al. 1997), and evidence for cycle-like variability in D_3 seen in multi-year stellar programs involving high-precision radial velocity monitoring (Santos et al. 2010). Although a stronger feature, for a long time, studies of the He I λ10830 line in late-type dwarf stars have been more limited due to the lack of sensitivity of available detectors in this spectral region, though probes of chromospheric structure based on λ10830 have been carried out in recent years with large-aperture telescopes (e.g., Takeda & Takada-Hidai 2011; Smith et al. 2012). To our knowledge, there are no near-simultaneous observations of both D_3 and λ10830 in stars displaying solar-like activity, while such data exist for T Tauri stars (e.g., Dupree et al. 2012).

The primary challenges in the utilization of the helium triplet lines are that (a) they are intrinsically weak and (b) they are blended with terrestrial water lines. These issues are best addressed with very high-quality spectra (in terms of signal-to-noise ratio (S/N) and resolution) acquired at very dry sites to mitigate the effects of terrestrial water vapor contamination. Even when these requirements are met, the presence of blends with nearby atomic lines in the stellar spectrum due to rotational smearing (which is typically larger in more active late-type stars) introduces an additional source of error in the estimates of equivalent width. In addition to the difficulties of observing each line individually, their wide wavelength separation adds further challenges in obtaining simultaneous spectra with the same spectrograph.

In view of these considerations, we utilized the 8.2 m Very Large Telescope (VLT) and the CRyogenic high-resolution InfraRed Echelle Spectrograph (CRIRES) at the European Southern Observatory (ESO) at Cerro Paranal to obtain the NIR λ10830 spectra on the night of UT 2011 December 6–7. The D_3 spectroscopic observations were carried out on the same night using the Fiber Extended-range Optical Spectrograph (FEROS), mounted at the 2.2 m Max-Planck Gesellschaft/European Southern Observatory (MPG/ESO) telescope at La Silla (Chile), during MPG guaranteed time.

3.1. Target Selection

The principal selection criteria for the stellar sample included visually bright ($V < 7$) F, G, and K dwarfs that are detected X-ray sources in the *ROSAT* All-Sky Bright Source Catalog

Table 1
Journal of Observations

HD	Sp. type[a]	$B-V$[a]	UT Start Time		Nod. pos.	Notes
			FEROS	CRIRES		
HD 49933	F3V	0.36	06:22:47			
			06:25:23			
			06:27:59			
HD 29992	F3IV	0.37	03:19:05	03:40:28	A	
			03:20:41	03:42:28	B	
			03:22:19			
HD 37495	F5V	0.46	05:07:55	05:10:26	A	No AO
			05:10:01	05:15:42	B	No AO
			05:12:07			
HD 27861	A1V	0.08	06:00:11	00:55:58	A	std
			06:02:23	00:58:43	B	std
			06:04:35			std
HD 18331	A1V	0.09	02:55:09			std
			02:57:31			std
			02:59:53			std

Note. The UT date for all start times is 2011 December 7. The label "std" in the notes indicates telluric standard.
[a] From the Bright Star Catalog (Hoffleit & Jaschek 1991) or the Simbad database.

(This table is available in its entirety in machine-readable form.)

(Voges et al. 1999) or listed in the Gliese–Jahreiss Catalog of Nearby Stars (Gliese & Jahreiss 1991). The application of the large-aperture VLT to bright objects served the dual objectives of efficiently obtaining spectra of the highest quality for a large number of targets in a single allocated night. The target selection criteria are clearly biased toward active stars since it was our intention to obtain spectra with detectable helium triplet lines in order to further develop our analysis methods as opposed to carrying out a survey at this time according to some completeness criteria.

The time differences between FEROS and CRIRES spectra of the same target are below 30 minutes, with the exception of HD 17051 and HD 33262 for which the time difference is about 1 hr. A journal of the observations is presented in Table 1. Note that the CRIRES observations at λ10830 terminated earlier due to the onset of adverse weather at the Cerro Paranal site, resulting in fewer targets observed than at the La Silla site where the D_3 spectra were obtained with FEROS and the ESO 2.2 m telescope. The details of the observations are given below.

3.2. FEROS Observations and Data Reduction

FEROS is a bench-mounted, thermally controlled instrument, fed by two fibers providing simultaneous spectra of either the object and wavelength calibration or the object and sky. It is designed to achieve high resolution ($R = 48{,}000$), high efficiency (≈20%), and to provide an almost complete spectral coverage from 3500 to 9200 Å spread over 39 echelle orders (Kaufer et al. 2000). The entrance aperture of the fiber has a projected diameter on the sky of 2.″0. As the cross-disperser is a prism, the spectral orders are strongly curved on the CCD. The detector is an EEV 2k4k CCD.

A total of 134 FEROS spectra of our targets (including telluric standards) were acquired using the object-sky mode to avoid contamination by Th–Ar lines, as for our purposes it was preferable to analyze clean spectra rather than attaining the highest radial velocity precision. The integration times of individual exposures ranged between 12 and 420 s to obtain an S/N greater than 200 for stars brighter than $V = 7$.

The data were reduced using a modified version of the FEROS Data Reduction System pipeline, implemented within ESO-MIDAS[8] (ver. 09SEPpl1.2) under context FEROS, which yields a wavelength-calibrated, normalized, one-dimensional spectrum. The details of the reduction steps are given by Schisano et al. (2009).

For each target, a triplet of consecutive spectra was obtained, with the exception of HD 88697. Pixels with unusually high values were identified by comparing the three spectra, and then flagged as missing. The triplet of spectra was then averaged to obtain a single spectrum with greater S/N. The estimated S/N in reduced spectra reach values of the order of 1000, with a mean value around 650.

3.3. CRIRES Observations and Data Reduction

The He I λ10830 spectroscopic observations were carried out in visitor mode on the same night as the FEROS D_3 observations, using CRIRES (Käufl et al. 2004, 2006), mounted at Unit Telescope 1 (Antu) of the VLT array at Cerro Paranal. The entrance slit width was set to 0.″2 to attain a nominal resolving power of $R = 10^5$. The CRIRES science spectra are recorded on an array of four 1024 × 512 Aladdin III detectors. The grating position (#52) was chosen so that the He I λ10830 line was recorded on detector #3. We verified that spectra on that detector were free of significant ghost features.

Each star was observed at two nodding offset positions along the slit, A and B, with jitter. The total exposure times of each science frame (without overhead) range from 2 to 10 s to obtain an S/N exceeding 200 for the target stars. Almost all of the science frames were obtained with the Adaptive Optics (AO) system on to optimize the S/N; only the last few spectra of the observing run were obtained with the AO off, because of the increasingly deteriorating seeing due to the onset of adverse weather, which eventually caused early termination of the run.

[8] Munich Image Data Analysis System.

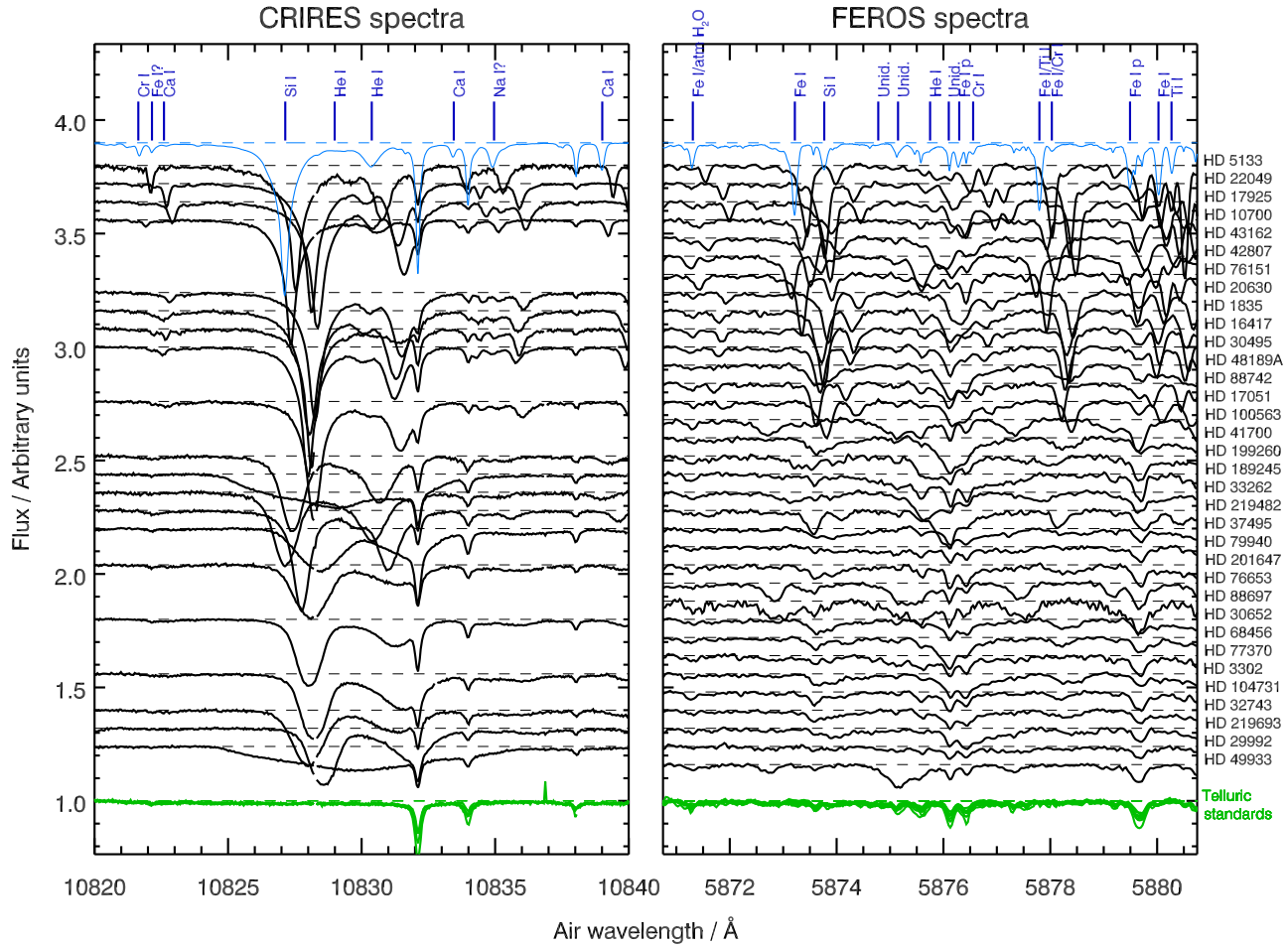

Figure 5. Target spectra around the wavelength regions of interest. Normalized fluxes are offset by a constant value. Spectra of telluric standards are shown at the bottom of the plot, highlighting the main telluric H_2O absorption lines in the range. The reference solar flux atlas by Kurucz et al. (1984) is also displayed for comparison as in Figure 2 with identification of the main solar lines in the range, from Swensson et al. (1970) and Moore et al. (1966).

Data reduction of each CRIRES frame was performed using the ESOREX pipeline for CRIRES. Science frames and flat-field frames were corrected for nonlinearity and 1D spectra were extracted from the combined flat-fielded frames with an optimal extraction algorithm. The wavelength solution is based on the Th–Ar calibration frames provided by ESO. The wavelength solution was then refined in the vicinity of the λ10830 line by matching the average positions of the strongest H_2O lines observed in the range 10772–10868 Å with the wavelengths given by Breckinridge & Hall (1973). The estimated S/N in the reduced spectra are in the range 200–700.

4. Spectral Analysis

After the data were reduced following standard instrument pipelines, we analyzed the 1D spectra around the wavelengths of interest (5876 and 10830 Å) using the Interactive Data Language (IDL). The spectra in these regions are shown in Figure 5. In both wavelength ranges, it was necessary to correct the object spectra for contamination by terrestrial lines by using the spectra of A stars obtained in the same observing run. Contamination by stellar blends also needed to be taken into account. In some cases, further uncertainties in the procedure are introduced by rotational smearing. Since the characteristics of telluric lines and stellar blends are different in the two wavelength ranges, the procedures for measuring the equivalent widths of the He I lines are slightly different, as described in detail in the following two sections. Examples of corrected spectra and of the fitted line profiles according to the procedures described in the following sections are shown in Figure 6. A summary of the results, together with the relevant stellar parameters, is given in Tables 3 and 4. In particular, we adopt the $v \sin i$ values given by Ammler-von Eiff & Reiners (2012), when available, or by Głębocki & Gnaciński (2005), with the exception of HD 48189A, for which the value given by Schröder et al. (2009) was adopted.

4.1. Measuring the D_3 Line

The He I λ5876 multiplet consists of six fine structure lines arising from the transitions between levels $1s\,2p\,^3P$ and $1s\,3d\,^3D$. The rest wavelength of the strongest component is at 5875.615 Å; four of the other components are separated at most by 25 mÅ from this component, while a sixth component, whose strength accounts for 1/9th of the total (exact value in LS coupling), is at 0.351 Å on the red side, giving a slightly asymmetric shape to the line in high-quality spectra.

The main difficulty in analyzing this line is that it is blended with a group of telluric H_2O lines at wavelengths of 5875.444, 5875.596, 5875.769, 5876.124, and 5876.449 Å, as listed by Moore et al. (1966). The procedure we adopted to correct for telluric blends relies on the observed spectra of telluric

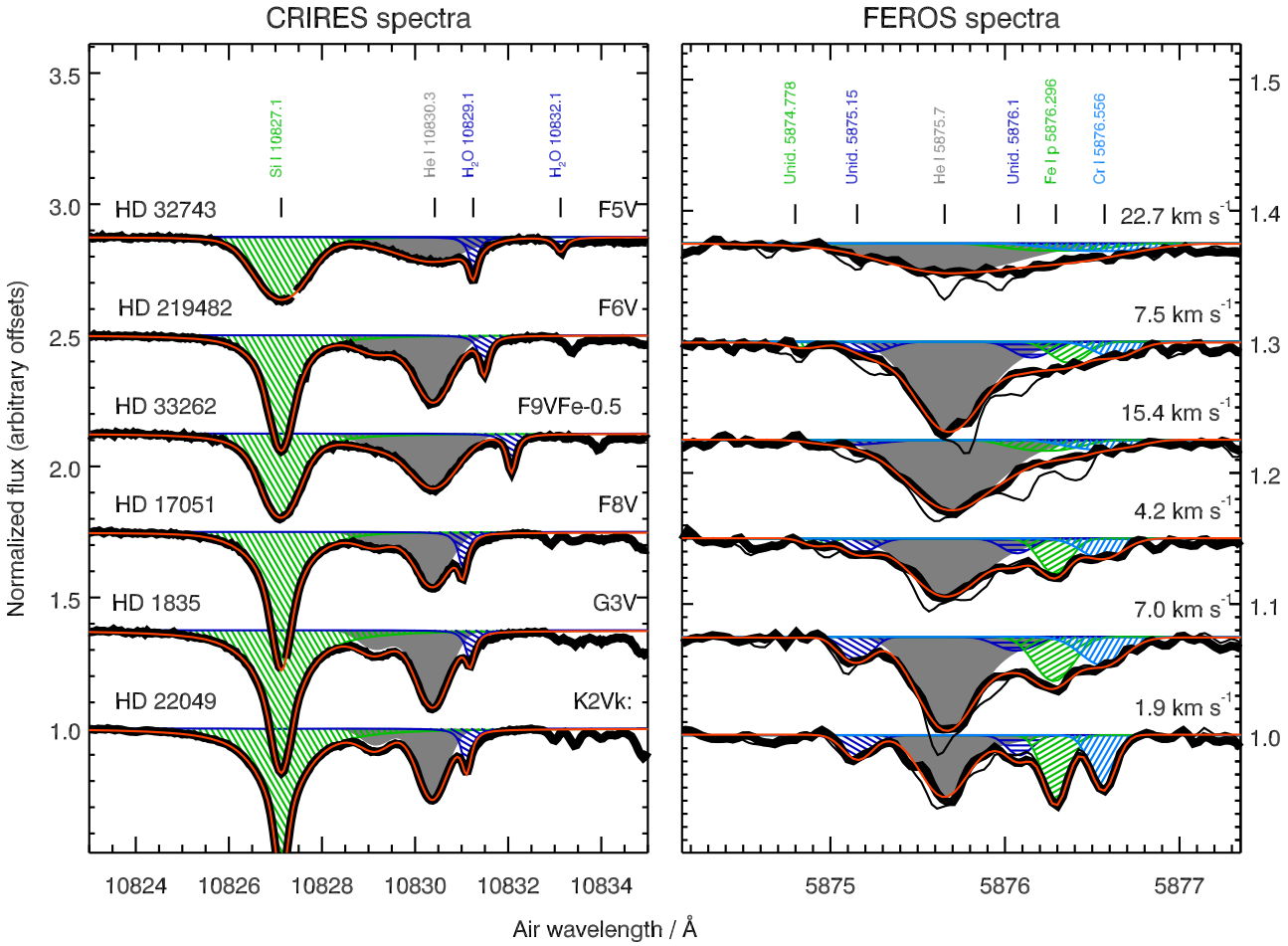

Figure 6. Examples of observed He I λ10830 (left) and λ5876 (right) profiles and their fit functions. Normalized fluxes are offset by a constant value. The fitted He I multiplets are highlighted by a solid gray area. The various nearby blends are highlighted by hatched areas. The total fit function is represented in red. In the panel showing the FEROS spectra, the thin solid line shows the spectra before the telluric correction. The spectral type and the $v \sin i$ value adopted to broaden the stellar lines are also indicated (in the right- and left-hand panels, respectively).

standards. Since the geometrical air mass inferred from the time of the observations is normally a poor indicator of the water vapor column mass for each spectrum, we chose instead to use as proxies the strongest H_2O lines in the range 5855–5930 Å, which appear to not be blended with stellar lines in all of the spectra. We found that the best proxy for this purpose is the sum of the equivalent widths of the H_2O lines at 5919.6, 5920.6, and 5925.0 Å. From the measured value of this proxy in each object spectrum, we derived the corresponding telluric spectrum by interpolating the spectra of the telluric standard pixel by pixel as a function of the proxy. This procedure of course ignores the details of the excitation of the individual H_2O lines and of all the other telluric lines. We estimated the error introduced by the telluric correction procedure on the λ5876 line at its rest wavelength and for $v \sin i = 0$ to be 1 mÅ rms or less; the error increases to 2.7 and 5.0 mÅ for profiles rotationally broadened by 40 and 80 km s^{-1}, respectively. Assuming the telluric correction to be proportional to the line broadening, we estimated its error correction as $\sigma_{\rm atm} = 0.89 + 0.047 \times v \sin i$, with $v \sin i$ in km s^{-1} and $\sigma_{\rm atm}$ in mÅ.

After the telluric spectrum was removed, we fitted the D_3 line profile with a composite profile of six Gaussians, each representing one of the fine structure components of the multiplet. The wavelength and Gaussian width of the reference component λ5875.615 were allowed to vary, while the wavelength separations and relative Gaussian widths of the other components were kept constant. The relative strengths were also kept constant at values proportional to the relative gf values. Thus, this composite profile for the λ5876 multiplet is still determined by only three free parameters (multiplet equivalent width, position, and width of the main component) as in standard, single-Gaussian fitting procedures. The multiple-Gaussian profile thus constructed was then broadened by the $v \sin i$ value given in the literature for each target (see Tables 3 and 4).

The solar line list compilation by Moore et al. (1966) reports the presence of at least three photospheric lines potentially affecting the measurement of the λ5876 equivalent width: Fe I λ5876.30, Cr I λ5876.45, and an unidentified line at 5874.778 Å. In several spectra, particularly in cooler stars, we also noticed at least two other unidentified lines at 5875.15 and 5876.1 Å (see Figure 5). All these lines can affect the determination of the equivalent width of the D_3 line for $v \sin i > 30$ km s^{-1}.

In nearly all of the spectra, we included some or all of those lines in the fit procedure as rotationally broadened Gaussians, adopting the $v \sin i$ value given in the literature. In spectra with significant rotational broadening, we constrained the wavelengths and in some cases, the Gaussian widths of the fitting

Table 2
Linear Fit Coefficients for Stellar Blends Near He I λ5876

Line	A_{B-V} (mÅ)	B_{B-V} (mÅ)	σ_{B-V} (mÅ)
Unid. λ5875.778	0.7	⋯	0.4
Unid. λ5875.15	−0.4	4.7	1.1
Unid. λ5876.1	0.9	1.8	0.7
Fe I λ5876.296	−1.8	12.9	1.8
Cr I λ5876.556	−1.3	9.4	1.3

functions within reasonable bounds to prevent unphysical results.

We found that these blends tend to increase toward cooler spectral types, thus confirming their stellar origin. Only the very weak 5874.778 Å blend does not exhibit an obvious trend with $B - V$. Table 2 reports the coefficients of the linear fit of the equivalent widths of these stellar blends, measured in mÅ, as functions of $B - V$ in the form $A_{B-V} + B_{B-V} \times B - V$, together with the standard deviation from the fit, σ_{B-V}. For those stars with high $v \sin i$ for which some or all of those blends could not be measured, the above relation can be used to estimate their contribution to the He I λ5876 equivalent width. In particular, we found that the equivalent widths of the Fe I λ5876.30 and Cr I λ5876.45 lines increase with $B - V$ from ∼2 mÅ at $B - V = 0.4$ to about ∼12 and ∼8 mÅ at $B - V = 1$, respectively.

Assuming a Poissonian noise model corresponding to the estimated S/N on the continuum, the resulting χ^2 of the fits are of the order of unity while the corresponding, formal uncertainties on the λ5876 multiplet equivalent width, $\sigma_{\rm fit}$, are less than 1 mÅ.

To estimate the effect of possible residual blends or of deviation from Gaussian profiles, we removed the fitted blending lines from the spectra. We then computed the equivalent width, $W_{\rm int}$, of the λ5876 multiplet by trapezoidal integration of the residual intensity. We estimated the uncertainty due to residual undetected blends or deviations from Gaussian profiles as $\sigma^2_{\rm nG} = (W_{\rm int} - W_{\rm fit})^2$, where $W_{\rm fit}$ is the equivalent width from the multi-Gaussian fit procedure described above. These differences are typically of the order of 1 mÅ, and in any case below 3 mÅ, even in the faster rotators.

We then estimated the overall uncertainty on the measured λ5876 equivalent width by summing quadratically the above estimates with the uncertainty due to the removal of the telluric spectrum: $\sigma^2_{\rm tot} = \sigma^2_{\rm fit} + \sigma^2_{\rm nG} + \sigma^2_{\rm atm}$. The He I λ5876 equivalent width and its associated uncertainty thus estimated are reported as W in the fifth column of Tables 3 and 4.

Finally, in those spectra for which not all of the stellar blends could be fitted, we took advantage of the estimated equivalent widths of those lines from the coefficients listed in Table 2. The sum of the blends falling within the He I λ5876 line profile but not explicitly fitted, along with their uncertainties (from a quadratic sum), is reported as $W_{\rm bl}$ in Tables 3 and 4. The equivalent width of the He I λ5876 multiplet obtained by subtracting this estimated contribution is reported as $W_{\rm corr}$.

4.2. Measuring the λ10830 Line

The He I λ10830 triplet arises from the transitions between levels $1s\,2s\,^3S$ and $1s\,2p\,^3P$. The two principal components are usually observed as a single line whose rest wavelength is at 10830.34 Å, since they are separated by only 90 mÅ; the third component is at 10829.09 Å and is therefore often resolved in solar and stellar spectra. In optically thin conditions, the *gf* value of this minor component is in the ratio 1:8 (exact value in LS coupling) relative to the sum of the other two components.

As in the case of the D_3 line, there are some nearby telluric H_2O lines that could interfere with the measurement of the equivalent widths of the line components (Swensson et al. 1970; Breckinridge & Hall 1973). The telluric line closest to the rest wavelength of the main component is at 10830.0 Å, but is so weak we were unable to detect it even in the spectra of the A-type telluric standards. The next closest, easily discernible H_2O line is at 10832.1 Å. Another H_2O line at 10834.0 Å, while fainter, also had to be taken into account in a few cases. These telluric lines were both fitted with two Gaussian profiles with fixed wavelengths.

The red wing of the nearby, strong Si I λ10827.14 Å line often affects the profile of the He I λ10830 triplet. The problem of treating this blend has been extensively discussed in the context of spatially resolved solar spectra (Giovanelli & Hall 1977; Jones 2003; Malanushenko & Jones 2004). In these high S/N spectra without evident velocity shifts, however, we found that the wings of the Si I line could satisfactorily be fitted by a Voigt profile. We also found that fits could be improved if the core of the Si I line is fitted separately with a Gaussian profile with the same central wavelength.

Finally, the He I λ10830 triplet was represented by three Gaussians at 10830.34, 10830.25, and 10829.09 Å whose wavelength separations and relative Gaussian widths were kept constant. The relative strengths of the components at 10830.34 and 10830.25 Å were also fixed at the 5:3 ratio of their *gf* values.

The fitting functions for the stellar lines were broadened using the $v \sin i$ value from literature (see Tables 3 and 4). In some spectra, the large value of $v \sin i$ prevented the independent fit of the strength of the He I minor component with respect to the other two; in this case, the relative strength of the He I λ10829.09 Å to the sum of the other two was fixed to the optically thin ratio of 1:8. In summary, the He I λ10830 triplet is fitted with a composite, multi-Gaussian profile with three or four free parameters: multiplet equivalent width, position and width of the main component, and when possible, the equivalent width of the minor component at 10829.09 Å.

As in the case of the FEROS spectra, we assumed a Poissonian noise model corresponding to the estimated S/N on the continuum. The resulting χ^2 of the fits are of the order of unity while the corresponding formal uncertainties on the λ10830 multiplet equivalent width, $\sigma_{\rm fit}$, are normally less than 3 mÅ, with some exceptions reaching 7 mÅ. In contrast with the determination of the D_3 equivalent width, the determination of the nearby stellar Si I line and the removal of the telluric H_2O lines do not dominate the error budget.

We however estimated the effect of possible residual blends or deviations from Gaussian profiles adopting the same approach as for the FEROS spectra. We thus obtained an estimate of the uncertainty due to residual undetected blends or deviations from Gaussian profiles as $\sigma^2_{\rm nG} = (W_{\rm int} - W_{\rm fit})^2$, from the spectra after the telluric and stellar blends were removed. These differences are below 10 mÅ (on average of the order of 5 mÅ). The only exception is HD 17925, probably due to a CN blend at 10831.37 Å included in the integration of the residual profile but effectively filtered out by the fit procedure. In the case of the He I λ10829.09 Å component, we

Table 3
Helium Equivalent Width Measurements and Data for Program Stars: $B - V \leqslant 0.5$

HD	$B - V$	$v \sin i$[a] (km s^{-1})	$\log L_X$[b] (erg s^{-1})	$W_{\rm fit}$(He I λ5876) (mÅ)	$W_{\rm corr}$(He I λ5876) (mÅ)	$W_{\rm bl}$(λ5876) (mÅ)	W(He I λ10830) (mÅ)	W(He I λ10829.1) (mÅ)	f(C)	f(C-np)	$f_{\rm min}$
HD 49933	0.36	9.9	29.50	27.6(1.4)	27.6(1.4)	…	…	…	…	…	…
HD 29992	0.37	97.5	28.83	27.1(5.5)	18.4(6.1)	8.7(2.6)	364.3(9.6)	…	…	…	0.88
HD 219693	0.39	19.9	28.98	30.1(1.8)	26.4(2.3)	3.7(1.4)	259.6(5.8)	38.5(5.1)	0.66(0.04)	0.72(0.03)	0.59
HD 32743	0.39	22.7	29.02	21.3(2.2)	18.3(2.5)	3.0(1.3)	184.2(4.2)	28.6(3.7)	0.44(0.04)	0.50(0.03)	0.39
HD 104731	0.41	15.9	28.49	14.1(1.7)	10.3(2.2)	3.8(1.4)	…	…	…	…	…
HD 3302	0.41	17.8	29.40	33.2(2.0)	30.1(2.4)	3.1(1.3)	305.0(6.0)	48.7(5.3)	0.83(0.05)	0.89(0.04)	0.72
HD 77370	0.42	60.4	29.07	23.2(4.6)	16.6(4.9)	6.6(1.9)	…	…	…	…	…
HD 68456	0.43	8.8	29.15	33.1(1.3)	31.4(1.5)	1.7(0.7)	…	…	…	…	…
HD 30652	0.44	17.3	29.03	20.8(2.0)	17.4(2.4)	3.3(1.3)	187.7(11.0)	31.6(9.1)	0.47(0.07)	0.52(0.06)	0.40
HD 88697	0.44	19.8	29.49	38.1(2.1)	34.1(2.5)	4.0(1.4)	…	…	…	…	…
HD 76653	0.45	10.3	29.33	28.8(1.4)	27.1(1.6)	1.7(0.7)	…	…	…	…	…
HD 201647	0.45	22.4	28.92	18.5(2.1)	14.5(2.5)	4.1(1.4)	174.7(9.1)	24.6(8.1)	0.45(0.07)	0.50(0.07)	0.36
HD 79940	0.45	117.2	28.79	28.5(6.9)	17.4(7.4)	11.0(2.6)	…	…	…	…	…
HD 37495	0.46	27.2	29.31	25.9(2.2)	21.7(2.6)	4.1(1.4)	290.2(8.6)	…	0.89(0.07)	0.92(0.05)	0.68
HD 219482	0.47	7.5	29.42	35.9(1.3)	35.9(1.3)	…	318.5(4.3)	62.6(3.6)	0.85(0.03)	0.91(0.02)	0.75
HD 33262	0.47	15.4	28.71	34.9(1.6)	33.1(1.8)	1.7(0.7)	317.2(4.3)	56.3(3.7)	0.86(0.04)	0.92(0.03)	0.75
HD 189245	0.49	72.6	29.90	76.9(5.3)	64.7(5.9)	12.2(2.6)	409.6(4.1)	…	…	…	1.00
HD 199260	0.50	13.7	29.18	31.4(1.8)	29.5(2.1)	1.9(1.1)	294.3(5.7)	51.5(4.9)	0.81(0.05)	0.87(0.04)	0.69

Notes.
[a] From Ammler-von Eiff & Reiners (2012) when available, otherwise from Głębocki & Gnaciński (2005).
[b] From Hünsch et al. (1999), except L_X for HD 49933, which is from Hünsch et al. (1998).

Table 4
Helium Equivalent Width Measurements and Data for Program Stars: $B - V > 0.5$

HD	$B - V$	$v \sin i$[a] (km s^{-1})	$\log L_X$[b] (erg s^{-1})	$W_{\rm fit}$(He I λ5876) (mÅ)	$W_{\rm corr}$(He I λ5876) (mÅ)	$W_{\rm bl}$(λ5876) (mÅ)	W(He I λ10830) (mÅ)	W(He I λ10829.1) (mÅ)	f(C)	f(C-np)	$f_{\rm min}$
HD 41700	0.52	14.7	29.63	45.6(1.6)	41.1(2.1)	4.5(1.4)	…	…	…	…	…
HD 100563	0.53	13.5	29.13	26.2(1.6)	21.6(2.1)	4.6(1.4)	…	…	…	…	…
HD 17051	0.57	4.2	28.83	24.2(1.1)	24.2(1.1)	…	239.0(1.4)	47.7(1.1)	0.66(0.03)	0.71(0.03)	0.54
HD 88742	0.59	2.7	28.58	15.8(1.0)	15.8(1.0)	…	…	…	…	…	…
HD 48189A	0.61	15.5	29.99	38.3(1.6)	35.8(2.0)	2.5(1.1)	…	…	…	…	…
HD 30495	0.64	2.9	28.83	19.8(1.0)	19.8(1.0)	…	223.6(5.7)	41.4(4.6)	0.72(0.08)	0.76(0.07)	0.50
HD 16417	0.66	2.5	27.81	4.5(1.2)	4.5(1.2)	…	71.7(9.0)	12.1(7.3)	0.23(0.18)	0.31(0.20)	0.09
HD 1835	0.66	7.0	28.99	33.2(1.2)	33.2(1.2)	…	323.7(5.8)	67.0(4.8)	0.92(0.04)	0.96(0.03)	0.77
HD 20630	0.67	4.5	28.89	27.4(1.1)	27.4(1.1)	…	279.0(4.8)	55.6(3.7)	0.82(0.05)	0.87(0.04)	0.65
HD 76151	0.67	2.4	28.33	12.6(1.0)	12.6(1.0)	…	…	…	…	…	…
HD 42807	0.68	3.6	28.68	24.1(1.1)	24.1(1.1)	…	…	…	…	…	…
HD 43162	0.68	5.5	29.13	31.5(1.2)	31.5(1.2)	…	…	…	…	…	…
HD 10700	0.72	1.8	26.30	3.2(1.2)	3.2(1.2)	…	51.6(3.0)	…	0.12(0.14)	0.19(0.15)	0.03
HD 17925	0.86	4.8	29.08	28.1(1.1)	28.1(1.1)	…	317.6(20.9)	70.0(16.0)	…	…	0.75
HD 22049	0.88	1.9	28.32	18.1(1.0)	18.1(1.0)	…	257.8(3.6)	51.3(3.0)	…	…	0.59
HD 5133	0.94	1.8	27.79	12.6(1.0)	12.6(1.0)	…	229.8(11.7)	42.3(9.6)	…	…	0.51

Notes.
[a] From Ammler-von Eiff & Reiners (2012) when available, otherwise from Głębocki & Gnaciński (2005) or (HD 48189A) from Schröder et al. (2009).
[b] From Hünsch et al. (1999).

scaled the corresponding estimate as $\sigma_{\rm fit}(\lambda 10829.09)/\sigma_{\rm fit}({\rm total})$. The overall uncertainties from the fit procedure listed in Tables 3 and 4 are then obtained as $\sigma^2_{\rm tot} = \sigma^2_{\rm fit} + \sigma^2_{\rm nG}$.

5. Results and Discussion

The list of objects with our equivalent width measurements of the triplet lines is given in Tables 3 and 4. In the case of the D_3 line, we report both the equivalent width measured as described in the previous section, $W_{\rm fit}$(He I λ5876), and the corrected value, $W_{\rm corr}$(He I λ5876), obtained after an estimate of the sum of residual, undetected stellar blends in the line profile is removed, also reported in those tables as $W_{\rm bl}(\lambda 5876)$. Additional properties of the stars that are relevant to this investigation are included in Tables 3 and 4, as well as the determination of filling factors, f, derived from Equation (1) for the two series of models we have considered, together with their estimated errors determined as described in Section 2 and illustrated in Figure 3. Tables 3 and 4 also list the minimum filling factors, $f_{\rm min}$, from Equation (2), obtained from the measurement of the λ10830 line only, using the values $W_{\rm q} = 40$ mÅ and $W_{\rm max} = 410$ mÅ discussed in Section 2.1.

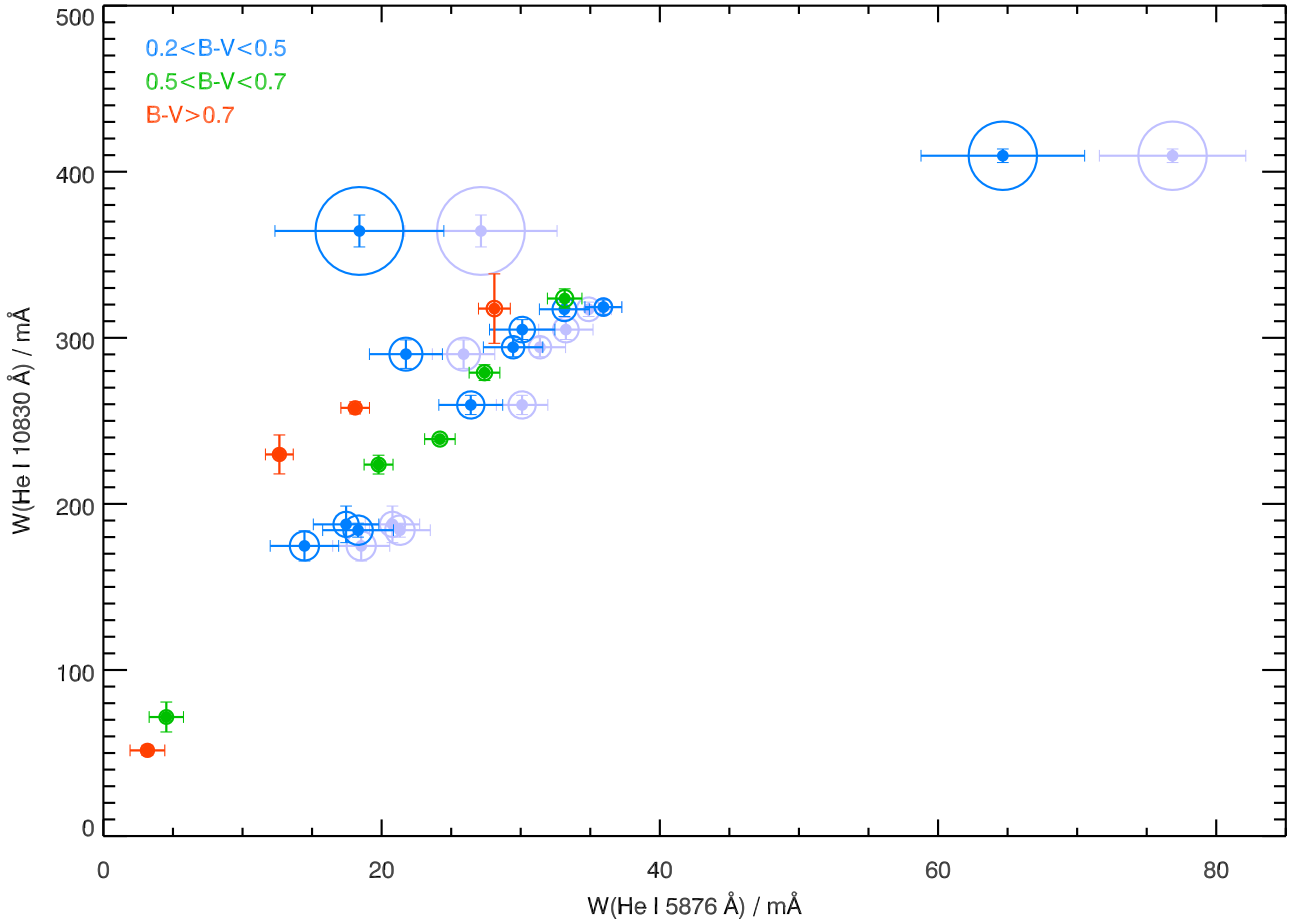

Figure 7. Observations of the He I triplet lines in solar-type stars. Error bars represent 1σ uncertainties, estimated as described in Section 4. Points with an outer circle represent stars with a projected rotational velocity exceeding 15 km s^{-1}; the radius of the circle is proportional to $v \sin i$. Ranges in $B - V$ are coded in colors. Points corresponding to the D_3 measurements not corrected for residual stellar blends, $W_{\rm fit}$(He I λ5876), are shown in lighter color. The general correlation between λ10830 and D_3 is evident in these data.

We display in Figure 7 the correlation between He I λ10830 and D_3 based on the data given in Tables 3 and 4. The data points corresponding to values $W_{\rm fit}$(He I λ5876), when different from $W_{\rm corr}$(He I λ5876), are shown in lighter colors. In the remainder of the discussion and in all the other figures, we will refer to $W_{\rm corr}$(He I λ5876) simply as W(He I λ5876). In both cases, the expected correlation between these diagnostics is evident in Figure 7 though there appears to be a saturation in the λ10830 feature at $W_{\lambda 10830} \approx 300$ mÅ. This saturation is also apparent in the correlation of λ10830 with X-ray luminosity as seen in the left-hand panel of Figure 8. This is precisely the behavior expected on the basis of the theoretical considerations discussed in Section 2. Likewise, the strength of the D_3 feature is directly correlated with X-ray luminosity although no saturation in this less optically thick line appears (right-hand panel of Figure 8). We note, parenthetically, that the correlations in Figure 8 with coronal X-ray emission levels are not only the direct result of a photoionization–recombination line formation process, as has been discussed by AG95 and AJ97 (also see Andretta et al. 1995), but also incidental to the generally elevated degree of magnetic activity and the corresponding enhanced average chromospheric and coronal pressures.

Figure 9 shows the correlation between the minor component of the He I λ10830 triplet and the sum of the other two main components at 10830.4 Å for those stars for which the minor component at 10829.1 Å could be fitted independently. In those cases, the ratio between the fine structure components range between 4 and 6, below the optically thin limit of 8, suggesting a significant optical thickness of the main component. These values of the line ratio are consistent with the stronger line profiles shown in Figure 2.

The measurements presented in Figure 7 may be compared to the calculated joint response of the two He I triplet lines as given in the left-hand panel of Figure 10. The results of the model calculations are given as loci of filling factors for two different series of scaled chromospheric models, C and C-np, described in Section 2.1 and shown in Figure 4.

With a few exceptions discussed below, the majority of these simultaneous observations of D_3 and λ10830 appear below the model loci for unit filling factor in panel (a) of Figure 10. In particular, the observed saturation in λ10830 follows the predicted behavior of the two lines. Note also that the error bars correspond to 1σ statistical uncertainties, and thus some of the points above the $f > 1$ loci are consistent with the theoretical estimates within 2σ or 3σ. We consider this as a confirmation that the approach is plausible, as already noted by AG95, by using less accurate, non-simultaneous data from the literature.

In particular, the relatively high fractional area coverages generally exceeding $f \sim 0.3$ are not surprising for active solar-type stars. On the other hand, exceptions occur in Figure 10 with apparently unphysical filling factors >1. The objects with

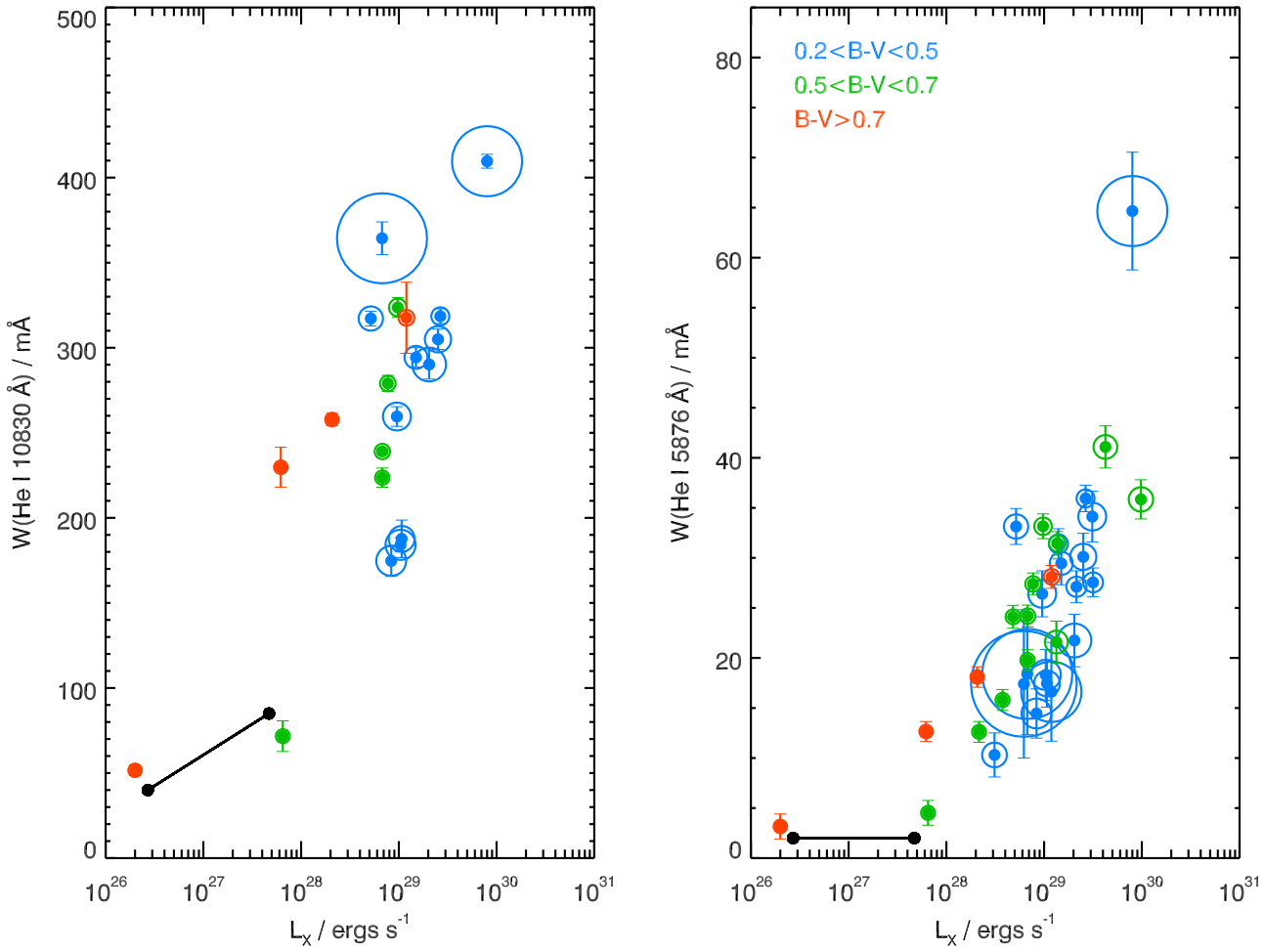

Figure 8. Strength of the individual triplet features vs. X-ray luminosity in our sample of solar-type stars. Left: the correlation between the equivalent width of λ10830 and coronal X-ray emission in this sample. Right: similarly for the D_3 line at 5876 Å. The range of variability of the X-ray luminosity of the Sun (Peres et al. 2000) and the corresponding Sun-as-a-star λ10830 equivalent widths (Harvey & Livingston 1994; Livingston et al. 2010) are also shown as a black segment. We adopted an upper limit for the λ5876 equivalent width of 2 mÅ. A possible saturation may be present in the λ10830–X-ray relationship. This is expected from the discussion of the origin of W_{max} for that line (Section 2).

$B - V > 0.8$ are K dwarfs for which our dwarf G chromospheric models may not apply. Specifically, the background radiation temperatures associated with the triplet transitions may be too high for K dwarf chromospheres, as discussed in Section 2.1. The dependence on T_{eff} of the joint response of the two lines is apparent in the optically thin limit shown both in Figures 4 and 10.

An analogous argument does not apply to the early F dwarf exceptions that are above the $f = 1$ locus in Figure 10 (HD 29992, HD 189245, and HD 37495), since the higher background photospheric radiation at 10830 Å would have the effect of increasing the gap between the data points and the $f = 1$ locus, although additional effects merit consideration in these cases. In particular, the procedure to account for undetected stellar blends described in Section 4.1 may be overcorrecting the strength of the D_3 in these relatively rapid rotators (see Figure 7). In addition, non-magnetic contributions to the triplet line strengths that include (a) a non-negligible photospheric contribution in these relatively warmer stars and (b) a contribution by acoustic heating due to the presence of more vigorous convective velocities. The former can be corrected through the application of appropriate photospheric models while the latter may yield insight into the role of acoustic heating in stellar chromospheres.

For each pair of equivalent width measurements falling within the allowed region of the (D_3, λ10830) plane, the corresponding pair of parameters (f, P/P_q) derived as described in Section 2 is shown in the right-hand panel of Figure 10. The results derived from the two adopted series of models, C and C-np, are shown with open and filled circles, respectively.

We recall that the adoption of the appropriate background photospheric model in the computation of the He I triplet lines would likely lower the equivalent width of the λ10830 line with respect to that for the D_3 feature. We would thus expect the theoretical joint response corresponding to $f = 1$ to fall closer to the observed data points for $0.2 < B - V < 0.5$. For these objects, therefore, the filling factors shown in the right-hand panel of Figure 10 are probably biased toward lower values.

In Figure 11 we apply the inferred filling factors to examine correlations relevant to dynamo modeling and chromospheric heating processes. In that figure, we note that the main uncertainty in determining the filling factor comes from the choice of the specific set of models, even neglecting the effect of the photospheric background described above. Thus, in the remainder of this paper we do not further discuss the errors shown in Figure 10 propagated from the observational

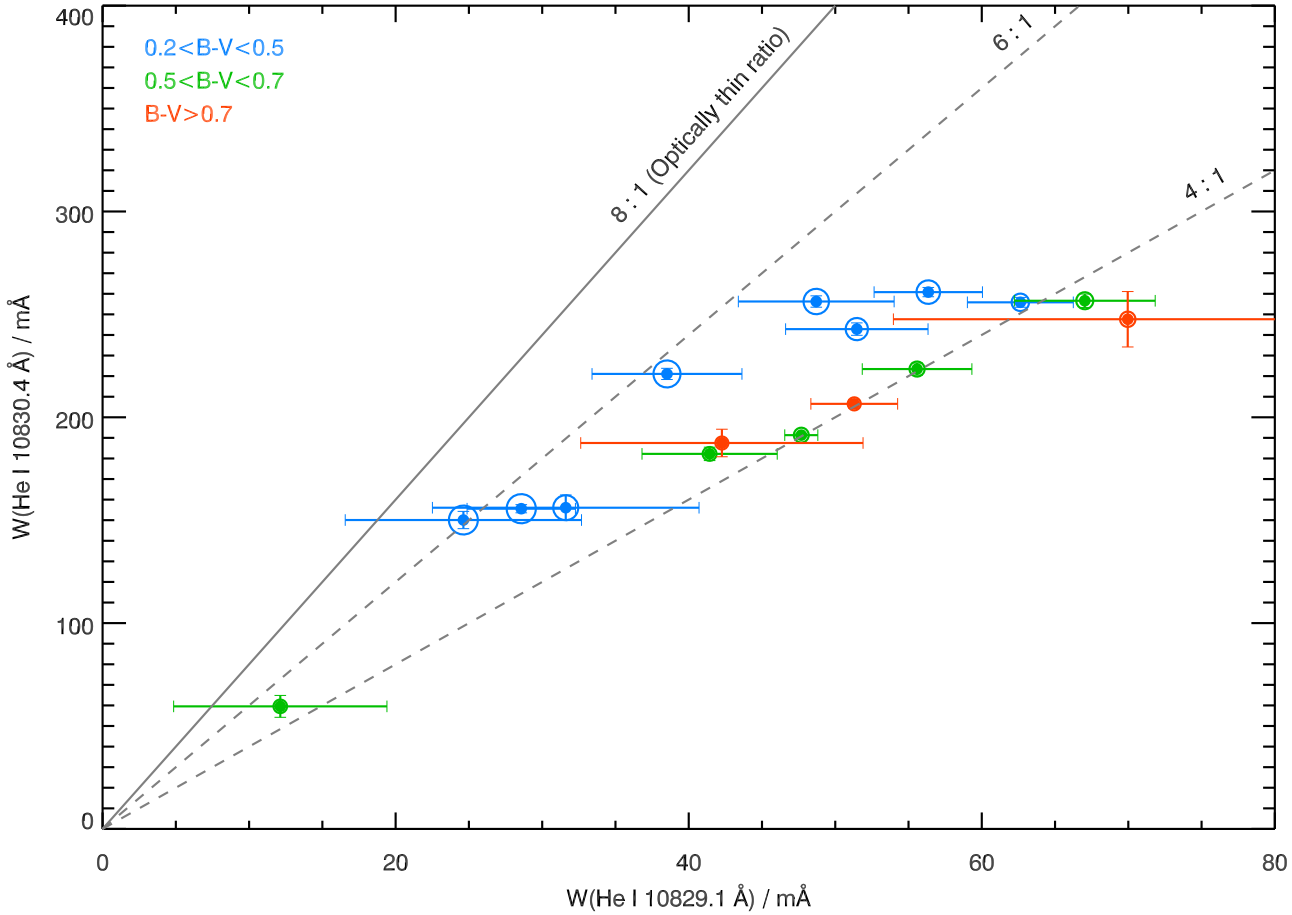

Figure 9. Correlation of the main components of the He I triplet at 10830.4 Å and the minor component at 10829.1 Å. The optically thin ratio (8:1) and two other representative values for the ratio of these fine structure components (6:1 and 4:1) are also shown.

uncertainties. On the other hand, since errors on rotational velocities can sometimes be substantial, we do show error bars on $v \sin i$ in panel (c). We have assumed that typical uncertainties are not smaller than 5% of $v \sin i$, with a lower limit of 1 km s^{-1} for $v \sin i < 20$ km s^{-1}. We adopted these lower limits if no larger uncertainty is specified in the source reference. We believe these lower limits are reasonable estimates because most of the uncertainties reported in $v \sin i$ measurements are of formal nature and do not normally reflect our knowledge on all broadening mechanisms involved.

Inspection of Figure 11 seems to indicate an interesting correlation between X-ray luminosity and the surface area coverage (panel (d)). We recall that Pizzolato et al. (2003) found the onset of saturation near $L_X \sim 10^{30}$ erg s^{-1} for solar-type stars in the broad range of rotation periods of $\sim$ a few to approximately 10 days. Our Figure 11(d) would suggest that this saturation may correspond to active region filling factors of $\sim$0.8–1.0.

A relation between the projected rotational velocity and active region filling factor in this small sample of stars is less evident (panel (c) of Figure 11). Nevertheless, in the case of cooler stars there is a trend of increasing filling factor with $v \sin i$. In the case of hotter stars, the trend seems to be the opposite, perhaps indicating a saturation of filling factors in the range 10–20 km s^{-1}. Once again, we cannot exclude a bias in the determination of f for these hotter objects.

The empirical correlation in the upper panels of Figure 11 merits further investigation because of its potentially important implications for the nature of chromospheric heating in active, solar-type stars. We have from Equation (1) for $W_q \approx 0$ that $f = W_{obs}/W_a(p)$, which yields a linear relation for a constant slope of $1/W_a(p)$. Consequently, the results in Figures 11(a) and (b) suggest that the intrinsic chromospheric heating in surface active regions in solar-type stars is similar. We indeed find that the activity parameters $p = P/P_q$ obtained by inverting Equation (1) for both λ5876 and λ10830 typically fall in the range of 10–30, i.e., the active region densities are about an order of magnitude higher than in the quiet Sun in the region of formation of the He I lines. A density contrast of this magnitude is consistent, for instance, with the model calculations by Fontenla et al. (2006) for solar plages and faculae. This result is clearly shown in the right-hand panel of Figure 10, where we highlight the narrow interval of chromospheric pressure within which the majority of the values fall. This interval of P/P_q is mapped in the relatively narrow region in the left-hand panel, which empirically corresponds to a near-linear joint response of the two He I lines.

The linear correlation of the two He I lines, when computed in stars with similar spectral type, is very tight. For stars with $B - V < 0.5$, excluding the fastest rotators ($v \sin i > 90$ km s^{-1}: HD 29992 and HD 189245), the standard deviation around the least-absolute-deviation linear fit of the relation λ5876 versus λ10830 is of only 3 mÅ. The λ5876 equivalent widths cover a range of 15–40 mÅ in this case. For stars with $0.5 < B - V < 0.7$, the standard deviation around the linear slope is even

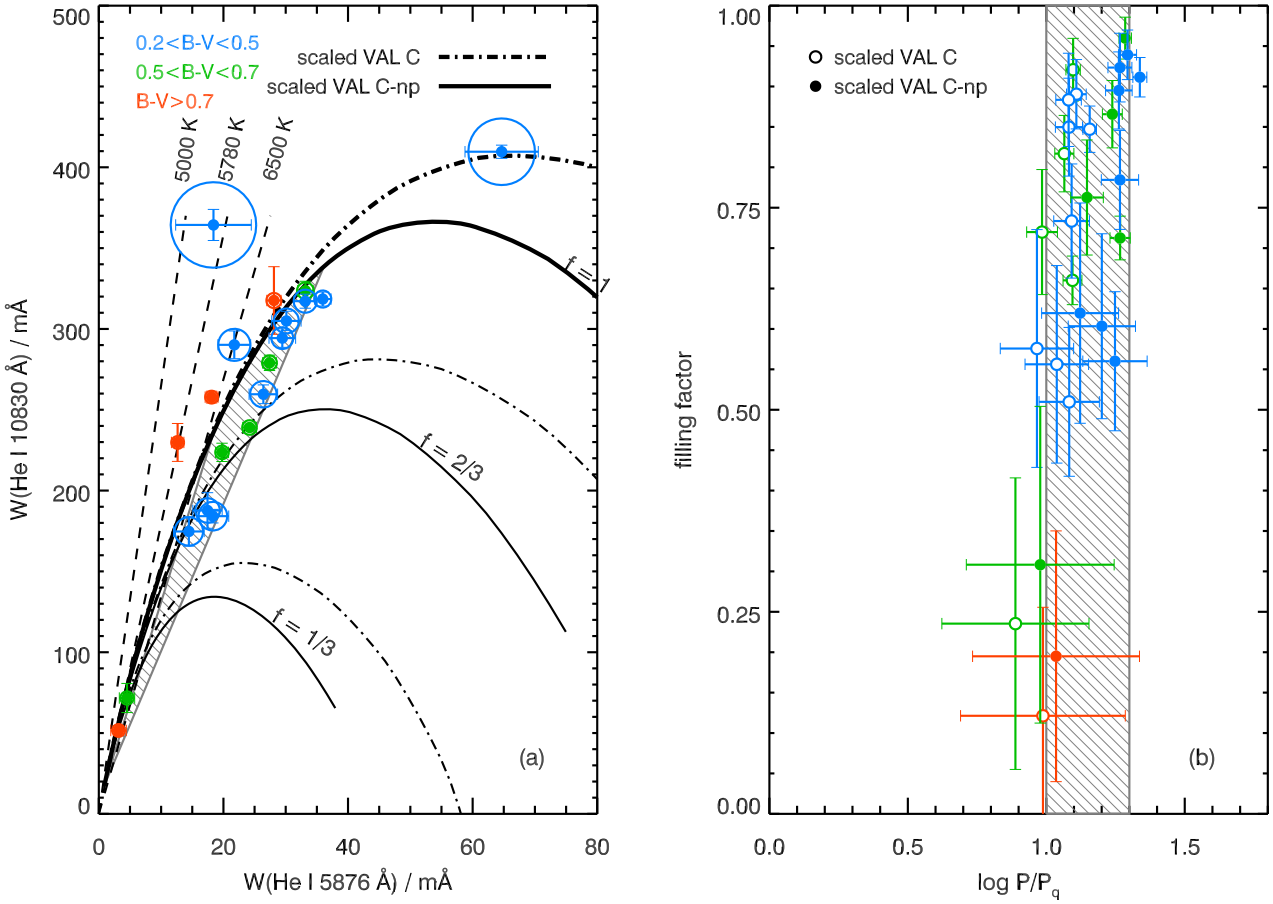

Figure 10. Filling factors and chromospheric mass loading atop the chromosphere from observed helium line strengths. Left-hand panel (a): loci of fractional active region area coverage, or filling factor, are superimposed on the observed strengths of the helium triplet lines as measured in this stellar sample. Data are represented with the same conventions as in Figure 7 while theoretical models are represented with the same conventions as in Figures 3 and 4. As in Figure 4, the optically thin limit of the joint response of the two lines as a function of stellar effective temperature is also shown. Right-hand panel (b): filling factors and mass loading atop the chromosphere (P/P_q) derived from the observed line strengths with the uncertainties estimated as described in Section 2. The open and filled circles represent results from the C and C-np model series. The dashed area in panel (b), corresponding to $1.0 < \log P/P_q < 1.3$, is also mapped in panel (a) in the case of the C-np series. See the text for a discussion.

smaller: about 1 mÅ; the range covered is 5–35 mÅ. The linear fit is relatively less good for stars with $B - V > 0.7$, with a standard deviation of 4 mÅ on smaller values of the D_3 line than in the other two groups of stars (5–25 mÅ). There are only four such stars in our sample, however.

This result would imply that the principal difference between chromospherically "active" stars and "quiet" solar-type stars is the surface filling factor of active regions. This is only a preliminary conclusion since the range in activity parameters for this small sample is comparatively narrow as measured by X-ray luminosity. However, we can add data from AG95 to extend the range, as illustrated in Figure 12. Although these data are non-simultaneous and generally of lower quality, they nevertheless support the linear trend in Figures 11(a) and (b). We also note that that there is evidence that indeed the variability with the solar cycle of the spectral irradiance in transition region lines (which are usually correlated with the optical He I lines) is mainly driven by the variability of the active region filling factor, not by changes in the intrinsic contrast with quiescent regions (Andretta & Del Zanna 2014).

With regard to the correlation between filling factors and rotational velocities, data for stars with $v \sin i < 10\,\mathrm{km\,s^{-1}}$ shown in Figure 12(c) seem to be consistent with the sharp increase shown in the corresponding diagram of Figure 11(c). In both cases, this trend is mostly due to cool stars with $B - V > 0.5$. On the other hand, it is less clear whether the decrease of the filling factor with $v \sin i$ above 20 km s^{-1} seen in Figure 11(c) can be supported by these lower quality, non-simultaneous measures.

Clearly, an enlarged stellar sample extending over a greater range of activity would be desirable before a firm conclusion can be established regarding the nature of non-radiative heating in active regions on solar-type stars. In this respect, it is unfortunate we could not complete the observations of all our program stars due to adverse weather. Furthermore, extending the solar theoretical models adopted here to a range of effective temperatures would help to reduce the uncertainties.

Measurements of these activity diagnostics at various epochs in the same star could be useful. But, if the tentative finding that the morphological differences in activity in solar-type stars are primarily due to the filling factor of otherwise similar active regions, then this would confirm the basic applicability of the solar paradigm to such objects. Moreover, this result is in contrast to what we find in the case of cooler dwarfs, namely, the M stars that are characterized by either Hα emission (i.e., dMe stars) or *chromospheric* Hα absorption. Since the Hα absorption feature in the spectra of dM (i.e., non-dMe) stars cannot be changed into an emission line simply by changing

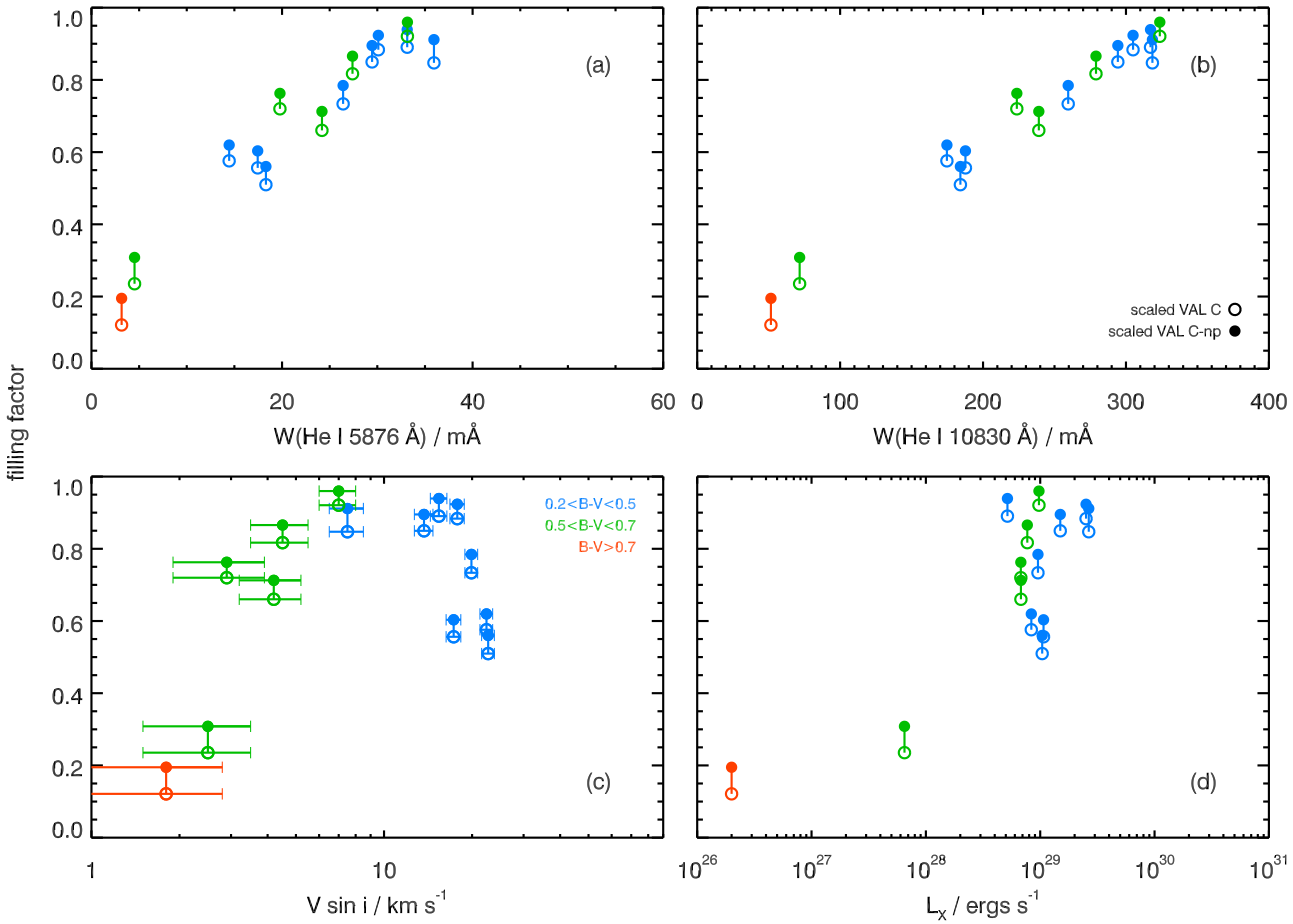

Figure 11. Calculated area coverage of active regions vs. observed line strengths and stellar parameters, respectively. The upper panels (a) and (b) show the inferred filling factor vs. the equivalent widths measured for each helium triplet line. Bottom panels: the deduced fractional area coverage vs. projected stellar rotational velocity (c) and X-ray luminosity (d). The open and filled circles represent the two results from application of the two chromospheric models utilized in this investigation, as indicated in the upper right panel and following the convention used in Figure 10. See the text for a discussion.

the filling factor of active regions alone, the differences between these stars in the context of magnetic activity must be due to differences in intrinsic chromospheric heating rates, and therefore, in the nature of the magnetic field-related energy dissipation in their atmospheres, at least at the level where the line forms.

6. Summary

Our results confirm and extend the previous work of AG95 with a set of simultaneously acquired spectra of exceptional quality for the principal objective of estimating the surface coverage of regions of significant magnetic flux emergence in solar-type stars outside of spots. We find that for most of the sample, the measured strengths of the He I triplet features in Figure 10 are below the locus of points corresponding to a filling factor of unity. In addition, the estimated filling factors given in Figure 11 (and the extension in Figure 12) suggest that the principal difference between active and quiet solar-type stars is due to the fractional area coverages of active regions rather than to a broad range of intrinsic non-radiative heating rates within active regions. This latter result would very naturally imply a linear relationship between the two He I lines distinct from the optically thin limit and parameterized by the filling factor (Equation (1)). A linear relationship between those two lines whose optical thicknesses are more than an order of magnitude apart would be difficult to explain with radiative transfer effects alone, independent of the specific chromospheric models adopted.

Although the observational results are broadly consistent with our modeling approach, exceptions are noted. We discuss these cases in the context of the need to apply a model atmosphere that is more appropriate to the stellar type, particularly for the cooler K dwarfs, and the possibility that non-magnetic contributions along with observational errors in the warm, very rapidly rotating F dwarfs in our sample could lead to effects not yet accounted for in the models that we applied.

The λ10830 line seems to be a particularly good indicator of filling factor. This may be understood from the fact that most of the observations fall just below the "flat" part of the λ10830 versus D_3 curves of joint responses in all of the atmospheric models we investigated. Hence, the joint behavior does not discriminate very well between different levels of "intrinsic" activity (parameterized by the chromospheric pressure), but the joint response does discriminate for the filling factor. The various classes of models only differ in the calibration of the relationship of $W_{\lambda 10830}$ versus f, but all indicate a good linear relationship between the two quantities.

The main difficulty in measurements of these features arises from the fact that the He I triplet lines are relatively weak features in the spectrum of solar-like stars. This is exacerbated by the presence of terrestrial water vapor blends and in some

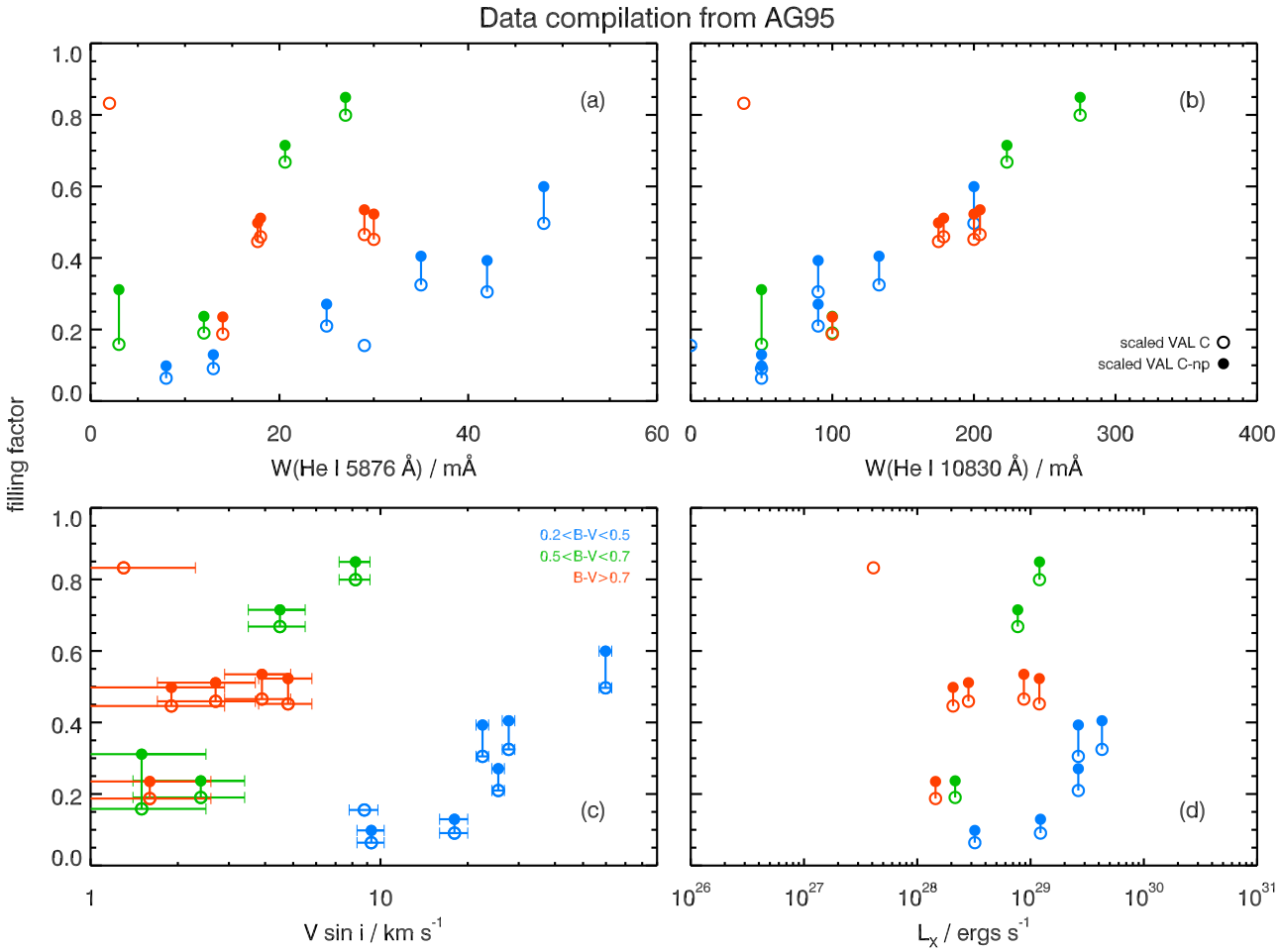

Figure 12. Same as Figure 11, from a previous data compilation of triplet helium line strengths. Previously acquired measures of λ5876 and λ10830 equivalent widths from AG95 for a different stellar sample are added to the data set discussed herein in order to extend the range of the correlation diagrams, in particular the correlation with X-ray luminosity. The scatter in the correlation diagrams is larger than in Figure 11 due to the lower quality and non-simultaneity of the data. Nevertheless, at least in panel (b) and—to a lesser extent—panel (a), the linear trends seen in that figure appear to be confirmed and extended to lower values of He I equivalent widths. The implication is that the intrinsic heating rates in active regions in solar-type stars are similar, with differences in the observed strength of the helium triplet feature due primarily to the area coverage of significant concentrations of magnetic flux. See the text for a discussion.

cases, by stellar blends that require careful corrections, especially for the D_3 line. Nevertheless, the range of applicability of this method can be extended to lower, more solar-like levels of activity as well as enhanced activity levels (typically correlated with rapid rotation) through high resolution, high S/N spectra obtained at sites characterized by very low humidity.

With our approach verified, we intend to obtain spectra for an expanded stellar sample. In parallel with the observational effort, we will develop a grid of chromospheric models as a function of effective temperature that can be applied to achieve improved discrimination between the possible loci of filling factors for a range of stellar types. In principle, the results from this total program could be used to determine for the very first time the empirical relationship between rotation and active region area coverage. Indeed, while correlations between rotation and radiative proxies of magnetic flux, such as Ca II or X-rays, have been determined for various stellar samples, the empirical relationship between actual magnetic active region area coverage and rotation has not been established.

Methods for independent verification of inferred active region filling factors may be pursued through other techniques such as Doppler imaging or by observations of eclipsing binaries. One novel approach is to obtain spectra of the helium triplet features during occultations of surface active regions by transiting exoplanets, specifically for systems with super-Jupiters in proximity to an active host star. In particular, signatures of exoplanet occultations of starspots have been observed with the high-precision photometry from the *CoRot* and *Kepler* missions (Wolter et al. 2009; Fraine et al. 2014). Analogously, distortions of the line profile in the form of relative increases or "bumps" should be seen in the triplet features in high-quality, time-resolved spectra, in analogy with spectroscopic signatures of transiting exoplanets described in, e.g., Mancini et al. (2015).

This work is based on observations collected at the European Organisation for Astronomical Research in the Southern Hemisphere with ESO Telescopes at the La Silla Paranal Observatory under program ID 088.D-0028(A) and MPG Utility Run for FEROS 088.A-9029(A). We are grateful to the ESO TAC and the Observatory technical support staff for supporting this program. We also thank Prof. Manfred Schüssler for valuable discussions in the definition phase of this project. Finally, we thank an anonymous referee for a

thorough reading of the manuscript and for comments that served to enhance the quality of presentation.

Facilities: ESO VLT (CRIRES), ESO MPG (FEROS), NSF McMath–Pierce (FTS), NSF SOLIS (VSM), NASA *SDO* (AIA).

Software: MIDAS, ESOREX, IDL.

References

Ammler-von Eiff, M., & Reiners, A. 2012, A&A, 542, A116
Andretta, V. 1994, PhD thesis, Univ. Naples "Federico II" (A94)
Andretta, V., & Del Zanna, G. 2014, A&A, 563, A26
Andretta, V., Del Zanna, G., & Jordan, S. D. 2003, A&A, 400, 737
Andretta, V., & Giampapa, M. S. 1995, ApJ, 439, 405 (AG95)
Andretta, V., Giampapa, M. S., & Jones, H. P. 1995, IrAJ, 22, 177
Andretta, V., & Jones, H. P. 1997, ApJ, 489, 375 (AJ97)
Andretta, V., Jordan, S. D., Brosius, J. W., et al. 2000, ApJ, 535, 438
Andretta, V., Mauas, P. J. D., Falchi, A., & Teriaca, L. 2008, ApJ, 681, 650
Baglin, A., Auvergne, M., Barge, P., et al. 2009, in IAU Symp. 253, Transiting Planets, ed. F. Pont, D. Sasselov, & M. J. Holman (Cambridge: Cambridge Univ. Press), 71
Baliunas, S. L., Donahue, R. A., Soon, W. H., et al. 1995, ApJ, 438, 269
Brault, J. W. 1979, MmArc, 106, 33
Breckinridge, J. B., & Hall, D. N. B. 1973, SoPh, 28, 15
Buzasi, D., Lezcano, A., & Preston, H. L. 2016, JSWSC, 6, A38
Cram, L. E., & Mullan, D. J. 1979, ApJ, 234, 579
Dupree, A. K., Brickhouse, N. S., Cranmer, S. R., et al. 2012, ApJ, 750, 73
Fontenla, J. M., Avrett, E., Thuillier, G., & Harder, J. 2006, ApJ, 639, 441
Fontenla, J. M., Avrett, E. H., & Loeser, R. 1993, ApJ, 406, 319
Fraine, J., Deming, D., Benneke, B., et al. 2014, Natur, 513, 526
García-López, R. J., Rebolo, R., Beckman, J. E., & McKeith, C. D. 1993, A&A, 273, 482
Giampapa, M. S. 1985, ApJ, 299, 781
Giampapa, M. S., Worden, S. P., & Linsky, J. L. 1982, ApJ, 258, 740
Giovanelli, R. G., & Hall, D. 1977, SoPh, 52, 211
Głębocki, R., & Gnaciński, P. 2005, yCat, 3244, 0
Gliese, W., & Jahreiss, H. 1991, in Preliminary Version of the Third Catalogue of Nearby Stars (CNS3), Vol. I, ed. L. Brotzmann & S. Gesser (Greenbelt, MD: NASA/Astronomical Data Center, GSFC), http://cdsarc.u-strasbg.fr/viz-bin/Cat?V/70A
Harvey, J., Krieger, A. S., Timothy, A. F., & Vaiana, G. S. 1975, MmArc, 104, 50
Harvey, J. W., & Livingston, W. C. 1994, in IAU Symp. 154, Infrared Solar Physics, ed. D. M. Rabin, J. T. Jefferies, & C. Lindsey (Dordrecht: Kluwer), 59
He, H., Wang, H., & Yun, D. 2015, ApJS, 221, 18
Hoffleit, D., & Jaschek, C. 1991, in The Bright Star Catalogue, ed. D. Hoffleit & C. Jaschek (5th ed.; New Haven, CT: Yale Univ. Obs.)
Hünsch, M., Schmitt, J. H. M. M., Sterzik, M. F., & Voges, W. 1999, A&AS, 135, 319
Hünsch, M., Schmitt, J. H. M. M., & Voges, W. 1998, A&AS, 132, 155
Jones, H. P. 2003, SoPh, 218, 1
Judge, P. G., & Pietarila, A. 2004, ApJ, 606, 1258
Kaufer, A., Stahl, O., Tubbesing, S., et al. 2000, Proc. SPIE, 4008, 459
Käufl, H. U., Amico, P., Ballester, P., et al. 2006, Msngr, 126, 32
Käufl, H.-U., Ballester, P., Biereichel, P., et al. 2004, Proc. SPIE, 5492, 1218
Koch, D. G., Borucki, W. J., Basri, G., et al. 2010, ApJL, 713, L79
Kurucz, R. L., Furenlid, I., Brault, J., & Testerman, L. 1984, Solar Flux Atlas from 296 to 1300 nm (Sunspot, NM: National Solar Observatory)
Lambert, D. L., & O'Brien, G. T. 1983, A&A, 128, 110
Landman, D. A. 1981, ApJ, 244, 345
Leenaarts, J., Golding, T., Carlsson, M., Libbrecht, T., & Joshi, J. 2016, A&A, 594, A104
Livingston, W., White, O. R., Wallace, L., & Harvey, J. 2010, MmSAI, 81, 643
MacPherson, K. P., & Jordan, C. 1999, MNRAS, 308, 510
Malanushenko, O. V., & Jones, H. P. 2004, SoPh, 222, 43
Mancini, L., Esposito, M., Covino, E., et al. 2015, A&A, 579, A136
Mauas, P. J. D., Andretta, V., Falchi, A., et al. 2005, ApJ, 619, 604
McQuillan, A., Mazeh, T., & Aigrain, S. 2014, ApJS, 211, 24
Moore, C. E., Minnaert, M. G. J., & Houtgast, J. 1966, The Solar Spectrum 2935 Å to 8770 Å, National Bureau of Standards Monograph 61 (Washington, DC: US Government Printing Office)
Muglach, K., & Schmidt, W. 2001, A&A, 379, 592
Nielsen, M. B., Gizon, L., Schunker, H., & Karoff, C. 2013, A&A, 557, L10
Peres, G., Orlando, S., Reale, F., Rosner, R., & Hudson, H. 2000, ApJ, 528, 537
Pietarila, A., & Judge, P. G. 2004, ApJ, 606, 1239
Pizzolato, N., Maggio, A., Micela, G., Sciortino, S., & Ventura, P. 2003, A&A, 397, 147
Reinhold, T., Reiners, A., & Basri, G. 2013, A&A, 560, A4
Saar, S. H., Huovelin, J., Osten, R. A., & Shcherbakov, A. G. 1997, A&A, 326, 741
Santos, N. C., Gomes da Silva, J., Lovis, C., & Melo, C. 2010, A&A, 511, A54
Sanz-Forcada, J., & Dupree, A. K. 2008, A&A, 488, 715
Schisano, E., Covino, E., Alcalá, J. M., et al. 2009, A&A, 501, 1013
Schröder, C., Reiners, A., & Schmitt, J. H. M. M. 2009, A&A, 493, 1099
Skumanich, A., Smythe, C., & Frazier, E. N. 1975, ApJ, 200, 747
Smith, G. H., Dupree, A. K., & Strader, J. 2012, PASP, 124, 1252
Smith, G. R. 2003, MNRAS, 341, 143
Smith, G. R., & Jordan, C. 2002, MNRAS, 337, 666
Swensson, J. W., Benedict, W. S., Delbouille, L., & Roland, G. 1970, Mém. Soc. R. Sci. Liège, Special Vol. 5
Takeda, Y., & Takada-Hidai, M. 2011, PASJ, 63, 547
Tobias, S. M. 1997, A&A, 322, 1007
Tu, J., & Song, P. 2013, ApJ, 777, 53
Vernazza, J. E., Avrett, E. H., & Loeser, R. 1981, ApJS, 45, 635
Voges, W., Aschenbach, B., Boller, T., et al. 1999, A&A, 349, 389
Wilson, O. C. 1978, ApJ, 226, 379
Wolff, S. C., Boesgaard, A. M., & Simon, T. 1986, ApJ, 310, 360
Wolff, S. C., & Heasley, J. N. 1984, PASP, 96, 231
Wolff, S. C., & Heasley, J. N. 1987, PASP, 99, 957
Wolff, S. C., Heasley, J. N., & Varsik, J. 1985, PASP, 97, 707
Wolter, U., Schmitt, J. H. M. M., Huber, K. F., et al. 2009, A&A, 504, 561
Yeo, K. L., Krivova, N. A., & Solanki, S. K. 2014, SSRv, 186, 137
Zarro, D. M., & Zirin, H. 1986, ApJ, 304, 365